

Durham Research Online

Deposited in DRO:

29 October 2010

Version of attached file:

Accepted Version

Peer-review status of attached file:

Peer-reviewed

Citation for published item:

Handley, H.K. and Macpherson, C.G. and Davidson, J.P. (2010) 'Geochemical and Sr-O isotopic constraints on magmatic differentiation at Gede volcanic complex, west Java, Indonesia.', Contributions to mineralogy and petrology., 159 (6). pp. 885-908.

Further information on publisher's website:

<http://dx.doi.org/10.1007/s00410-009-0460-z>

Publisher's copyright statement:

The original publication is available at www.springerlink.com

Additional information:

Use policy

The full-text may be used and/or reproduced, and given to third parties in any format or medium, without prior permission or charge, for personal research or study, educational, or not-for-profit purposes provided that:

- a full bibliographic reference is made to the original source
- a [link](#) is made to the metadata record in DRO
- the full-text is not changed in any way

The full-text must not be sold in any format or medium without the formal permission of the copyright holders.

Please consult the [full DRO policy](#) for further details.

1
2
3
4
5
6
7
8
9
10
11
12
13
14
15
16
17
18
19
20
21
22
23
24
25
26
27
28
29
30
31
32
33
34
35
36
37
38
39
40
41
42
43
44
45
46
47
48
49
50
51
52
53
54
55
56
57
58
59
60
61
62
63
64
65

1
2
3
4
5
6
7
8
9
10
11
12
13
14
15
16
17
18
19
20
21
22
23
24
25
26
27
28
29
30
31
32
33
34
35
36
37
38
39
40
41
42
43
44
45
46
47
48
49
50
51
52
53
54
55
56
57
58
59
60
61
62
63
64
65

Geochemical and Sr-O isotopic constraints on magmatic
differentiation at Gede Volcanic Complex (GVC), West Java,
Indonesia

Heather K. Handley*, Colin G. Macpherson, Jon P. Davidson
Department of Earth Sciences, Durham University, Durham, DH1 3LE, UK.

*Corresponding author. GEMOC Key Centre, Department of Earth and Planetary Sciences,
Macquarie University, Sydney, NSW 2109 Australia. Telephone: +61 2 9850 4405. Fax: +61
2 9850 8943. Email: hhandley@science.mq.edu.au

Abstract

The Gede Volcanic Complex (GVC) of the Sunda island arc (West Java, Indonesia) consists of multiple volcanic centres and eruptive groups with complex magmatic histories. We present new petrological, mineralogical, whole-rock major and trace element, and Sr-O isotopic data to provide constraints on the relative importance of fractional crystallisation and magma mixing in petrogenesis, as well as on the role and nature of the arc crust. Banded juvenile scoria from Young and Old Gede provide unequivocal evidence for the (late-stage) interaction of distinct magmas at Gede volcano. However, the relatively small-degree compositional zoning observed in plagioclase phenocrysts of all eruptive groups (up to ~20 mol% An) may be attributed to physical changes in magma properties (e.g. P , T , and PH_2O) rather than changes in melt composition. Major element and trace element variations within each eruptive series are inconsistent with magmatic evolution through simple mixing processes. Instead, mixing of variably fractionated magma batches is suggested to account for the significant scatter in some element variation diagrams. No correlation is observed between textural complexity and/or mineral disequilibrium and whole-rock geochemistry. REE data and geochemical modelling indicate that fractional crystallisation involving amphibole in the mid- to lower crust, and fractionation of plagioclase, clinopyroxene, Fe-Ti oxide \pm olivine \pm orthopyroxene provide strong control on the geochemical evolution of GVC rocks. Two-pyroxene geothermobarometry provides pre-eruption crystallisation temperatures of 891-1046°C and pressures of 3.4-6.5 kbar, equivalent to ~13-24km depth beneath the volcanoes (mid- to lower crust). Low, mantle-like clinopyroxene $\delta^{18}O$ values of GVC lavas and poor correlation of Sr isotope ratios with indices of differentiation precludes significant assimilation of isotopically distinct crust during magmatic differentiation. Therefore, we suggest that the geochemical character of the moderately thick West Javan arc crust is relatively immature compared to typical continental crust. Trace element ratios and strontium isotopes show that the magmatic source composition of the older geographical units, Gegerbentang and Older Quaternary, is distinct from the other GVC groups.

Key words

crustal contamination, fractional crystallisation, geochemistry, magma mixing, Sunda arc

Introduction

1 Arc lavas display a wide variation in composition, which reflects both the composition of the
2 primary magma from which they originated and the multitude of differentiation processes
3 magmas experience en route to the Earth's surface. Among the latter processes, fractional
4 crystallisation (Ewart 1982; Foden 1983; Gerbe et al. 1992), crustal contamination (Davidson
5 et al. 1987; Hildreth and Moorbath 1988; Davidson and Harmon 1989) and magma mixing
6 (Gamble et al. 1999; Tepley et al. 2000) are commonly called upon to explain geochemical
7 variation in arc lavas. Constraints upon the relative importance of differentiation processes at
8 individual volcanoes are essential before the characteristics of the source can be investigated.

9 The Sunda arc, formed by subduction of the Indo-Australian Plate beneath the
10 Eurasian Plate, includes around 80% of Indonesia's active volcanoes - many of which have
11 produced eruptions that have had significant impact on local and global environments (e.g.
12 Toba, Krakatau and Tambora). However, despite an apparently simple tectonic setting,
13 understanding magma genesis and evolution at the Sunda arc is complicated by along-arc
14 changes in the composition and thickness of the overriding Eurasian plate (Hamilton 1979).

15 GVC in West Java has been largely overlooked by petrologists and geochemists
16 studying petrogenesis of Sunda arc volcanoes. This is surprising considering the active Gede
17 Volcano (from which the complex derives its name) is one of the most prominent in West
18 Java and is located in close proximity (~70 km) to the densely populated capital, Jakarta.
19 Furthermore, to the east of GVC researchers have argued that the dominant crustal
20 component identified in magma genesis is provided by the subducting slab (i.e. source
21 contamination) (Edwards 1990; Gerbe et al. 1992; Turner and Foden 2001; Gertisser and
22 Keller 2003; Handley et al. 2007; cf. Chadwick et al. 2007), while to the west of GVC, He
23 (Gasparon and Varne 1998), Nd (Turner and Foden 2001) and Sr (Handley et al. 2008a)
24 isotopic investigations reveal the importance of shallow-level crustal contamination.
25 Therefore, GVC is in an ideal location to investigate contributions from the arc crust in
26 volcanic petrogenesis and conclusions from this study will help elucidate the nature of the
27 local arc crust. This paper presents new data on the petrography, mineralogy, geochemistry
28 and Sr-O isotopic composition of GVC volcanic products. Textural and chemical information
29 of phenocrysts is integrated with major, trace element and isotopic data to provide constraints
30 on the relative roles of fractional crystallisation and magma mixing, as well as the role and
31 possible nature of the arc crust. These questions are fundamental to understanding the
32 functioning of magmatic systems.

Geological setting

GVC is located in West Java within the Quaternary volcanic front of the Sunda arc (Fig. 1 inset). The Sunda arc forms the western part of the Indonesian subduction zone system and formed as a result of the northward subduction of the Indo-Australian Plate beneath the Eurasian Plate. A detailed tectonic description of the area is given by Hamilton (1979). GVC is dominated by the twin stratovolcanoes of Gede (2958 m), the only active volcano of the complex, and Pangrango (3019 m), an extinct volcano to the northwest (Fig. 1). Gede is divided morphologically and stratigraphically into Old and Young Gede (Situmorang and Hadisantono 1992). The remnant crater rim (50-200m high) of Old Gede is marked by Gunung Gumuruh (Fig. 1). This crater, now truncated by Young Gede in the north-west, is the largest (~1600m in diameter) and oldest crater at Gede. The volcanic deposits of Old Gede are exposed on the south-eastern slope of Gede and form a deeply dissected morphology. Young Gede consists of several smaller craters (Sela, Ratu, Lanang, Wadon and Baru) contained within the 1km wide, steep-walled (200m) Gede crater. Most of the eruptive deposits of Young Gede are confined in relatively narrow belts, extending north-east and south-west of the summit due to the topographic highs of Pangrango-Masigit and Old Gede in the northwest and southeast, respectively. The heavily forested Pangrango volcano is constructed on the north-east rim of a large caldera/collapse structure (Gunung Masigit, Fig. 1) which is open to the south-west. The Gegerbentang Complex consists of a series of eroded volcanoes situated to the north of Gede and is relatively older than both Gede and Pangrango (Fig. 1). The oldest deposits of Quaternary volcanic material (Older Quaternary Volcanic group) are exposed to the east and south west of Gede (Besar and Koncana respectively, Fig. 1). Basement rocks of the complex and surrounding area are dominated by Tertiary aged volcanogenic and marine sediments (Effendi et al. 1998). Around 20 small eruptions of short duration have been reported from Gede volcano since the mid-18th century. Pyroclastic flows were generated during a larger eruption in 1840. More recently, a brief ash ejection occurred in 1957 (VSI) and at the end of April 1991 a series of volcanic earthquake swarms were recorded (VSI). Kawah Lanang and Kawah Wadon are the most active craters at present, showing signs of hydrothermal activity.

Sample selection and grouping

The diverse range of volcanic rocks and volcanic related products from the GVC include: lava, pyroclastic flow, air fall, debris flow and lahar deposits. Sample material collected for

1 geochemical analysis was limited to fresh samples of lava flows and juvenile scoria from
2 pyroclastic flow deposits. The generally low LOI values for most samples (Table 1) and lack
3 of visible alteration in rock samples and thin sections (except in a few specimens) confirm the
4 samples are fresh. In this study the eruptive products of Young Gede are grouped into Young
5 Gede Kawah Ratu (those sourced from Kawah Ratu) and Young Gede Other Vents (sourced
6 from the Gede crater in general) due to uncertainty in the provenance of some samples and
7 the distinction of these two groups on the geological map of the Gede Volcanic Complex
8 (Situmorang and Hadisantono 1992). Here the term Pangrango refers to all units of the
9 Pangrango-Masigit centres and likewise, Gegerbentang, refers to all volcanic units within the
10 Gegerbentang complex. The relative stratigraphy of the volcanic centres and eruptive groups
11 is shown on the inset diagram in Fig. 1. On the basis of Ba/La and Zr/Nb trace element ratios
12 versus $^{87}\text{Sr}/^{86}\text{Sr}$ isotopes (Figs. 2a and b) volcanic rocks from Gegerbentang and the Older
13 Quaternary volcanics group are thought to represent a different geochemical source
14 composition and therefore these samples are highlighted (by contour lines) in subsequent
15 scatter diagrams. The analytical techniques used are given in the Supplementary data section.

16 Results

17 Petrography

18 The volcanic products of GVC have not been previously described. Therefore, this section
19 will focus on the petrography and mineralogy of each eruptive centre (in stratigraphical order
20 from the youngest to oldest) highlighting textural features which may contribute to the
21 understanding of petrogenesis at GVC. Basaltic andesite is the most common rock type
22 erupted and basalts are largely restricted to eruptives of Pangrango and Gegerbentang. The
23 majority of GVC rocks contain similar mineral assemblages of plagioclase, clinopyroxene
24 and Fe-Ti oxide \pm orthopyroxene \pm olivine. Petrographic summaries of Gede lavas are given
25 in Supplementary Table 1 and mineral data are found in Supplementary Tables 2-6.

26 Volcanic rocks from the Kawah Ratu centre of Young Gede (YGKR) consist of
27 basaltic andesites and andesites and contain a mineral assemblage of plagioclase,
28 clinopyroxene, orthopyroxene and Ti-magnetite, set within a very fine-grained groundmass of
29 plagioclase, Fe-Ti oxide and devitrified glass. The Kawah Ratu eruptives are dominantly
30 seriate in texture and contain the most textural complexity of all groups. Oscillatory zoning,
31 sieve textures and concentric bands of melt inclusions are observed in a large number of
32

1 plagioclase phenocrysts and microphenocrysts. More than half of the samples of this group
2 contain anhedral orthopyroxene phenocrysts mantled by clinopyroxene.

3 Rocks erupted from the Other Vents Group at Young Gede are dominated by basaltic
4 andesites, with minor andesites and contain an identical mineral assemblage to the Kawah
5 Ratu rocks, with the exception of olivine instead of orthopyroxene phenocrysts in a few
6 basaltic andesite samples. Rocks of this group display mainly porphyritic textures and are
7 generally less phenocryst rich than Kawah Ratu volcanic rocks and the plagioclase
8 phenocrysts are texturally less complex. Many of the rocks sampled of this group are highly
9 vesicular juvenile scoria of pyroclastic flow deposits, which contain a very fine-grained
10 groundmass of devitrified glass and plagioclase, or plagioclase, oxide and pyroxene. These
11 samples show evidence of magma mingling between dark, less evolved material and lighter
12 more evolved material (described in more detail below). Xenoliths of igneous origin are
13 present in some Young Gede samples (see below).

14 The basaltic andesites and andesites of Old Gede are dominantly porphyritic to seriate
15 in texture. In the basaltic andesites, plagioclase, clinopyroxene and titanomagnetite are
16 accompanied either by olivine, orthopyroxene or in a few cases both (suggestive of mineral
17 disequilibrium). Olivine is not present in the andesites. The volcanic products of Old Gede
18 contain lower modal abundances of ferromagnesian minerals compared to those of Young
19 Gede (Supplementary Table 1). The very fine- to fine-grained groundmass contains
20 plagioclase and oxide \pm pyroxene. Magma mingling textures are also observed in juvenile
21 scoria of pyroclastic flow deposits of this group (see below).

22 Eruptives from Pangrango consist of basalts and basaltic andesites. Most of these
23 lavas are strikingly porphyritic in hand specimen, containing large (up to ~1.2 cm) euhedral
24 clinopyroxene phenocrysts. The rocks are seriate in texture and mineral assemblages
25 comprise plagioclase, clinopyroxene, Ti-magnetite with either olivine (in the basalts) or
26 orthopyroxene (in the basaltic andesites). The phenocrysts are set in a fine-grained
27 groundmass of plagioclase, clinopyroxene \pm olivine. Some of the orthopyroxene phenocrysts
28 are mantled by clinopyroxene.

29 Most rocks from Gegerbentang display seriate textures of plagioclase, clinopyroxene,
30 orthopyroxene, with minor Ti-magnetite and rare olivine, in a very fine-, to fine-grained
31 groundmass of plagioclase and oxide \pm pyroxene.

32 It has proved difficult to obtain fresh samples from the Older Quaternary units;
33 chlorite is commonly observed replacing ferromagnesian minerals in these rocks and LOI
34 values are generally higher than those of other GVC rocks (0.35-0.91 wt%, Table 1). The

rocks contain the typical GVC mineral assemblage of plagioclase, clinopyroxene, orthopyroxene and Ti-magnetite. Minor hornblende is present within one sample, where it has been altered to biotite.

Mineral characteristics and chemistry

Plagioclase

Subhedral to euhedral plagioclase dominates the modal phase assemblage of all GVC rocks. Oscillatory zoning, sieve textures and concentric bands of melt inclusions are present in a large number of phenocrysts within all groups but particularly within Kawah Ratu rocks suggesting complex histories of these phenocrysts. In some Kawah Ratu samples, sieve-textured phenocryst cores are surrounded by clear rims of plagioclase. A large number of plagioclase phenocrysts in Young Gede and Old Gede rocks have irregular/patchy, pale brown, isotropic glass inclusions. Resorbed cores are present in occasional plagioclase phenocrysts from Pangrango and Kawah Ratu.

Plagioclase phenocrysts of GVC rocks display a broad range in composition from ~An₄₅-An₉₅ and are displayed in Figs. 3a-c. In the Young Gede Kawah Ratu rocks, compositions are more restricted in the basaltic andesites (An₆₈₋₈₆) than in the andesites (An₄₉₋₈₃, Figs. 3b and c, respectively), which display highly variable core, mid and rim anorthite contents. Plagioclase phenocrysts and groundmass An compositions in the basaltic andesites of the Young Gede Other Vents group display an extremely restricted range and are noticeably higher than those in other GVC groups (above 81 mol% with the exception of one rim sample, Fig. 3b), including the basalts from Pangrango (Fig. 3a). Plagioclase cores of the andesites lie within the range of basaltic andesite plagioclase cores of the Young Gede Other Vents group. However, mid and rim compositions extend to significantly lower Anorthite content (An₄₄). Plagioclase compositions cover a relatively broad range in both the basaltic andesite and andesites of Old Gede (Figs. 3b and c). Rim analyses of plagioclase in the basaltic andesites display a wide variation and extend to much higher An contents than groundmass analyses (An₅₂₋₅₇, Fig. 3b). Plagioclase compositions in rocks from Gegerbentang extend from moderate to high anorthite contents (An₅₉₋₉₀) with a reasonably wide range in core and rim composition when compared with mid sections of phenocrysts (Fig. 3b). In the Older Quaternary group, compositions are reasonably An poor (47-63 mol%) and phenocryst cores possess some of the lowest An contents (47-49 mol%) of GVC, with rim and mid sections displaying generally higher An contents (52-63 and 47-60 mol% respectively, Fig. 3c).

Compositional variations in An content from the core to rim of individual plagioclase phenocrysts are shown in Figs. 3d-f (open squares) and highlight reverse or normal zoning trends (see arrows Fig. 3d). The majority of GVC rocks display increases or decreases of ≤ 10 mol% An. All core- to rim variation amplitudes are within 20 mol% An, apart from the YGOV andesite (Fig. 3f), where the difference between the core to rim is ~ 40 mol% An (normal zoning). Reverse zoning trends showing greater than 10 mol% An variation between core and rim are only observed for the Older Quaternary andesite (Fig. 3f). The range in plagioclase core compositions within each sample is relatively limited (~ 1 -10 mol% An) except for basaltic andesites of Old Gede and Gegerbentang and a YGKR andesite, which display variations between adjacent plagioclase cores of ~ 20 -25 mol% An.

Clinopyroxene

Clinopyroxene (augite) is the most abundant ferromagnesian mineral (by modal volume) in GVC rocks, found in all samples accompanied by either olivine or orthopyroxene and very occasionally both (indicating mineral disequilibrium in the latter case). Phenocrysts are typically subhedral to euhedral and most exhibit simple twining, although oscillatory zoning is observed in some crystals. The phenocrysts display a broad range in size from microphenocryst to ~ 1.2 cm. Large (0.5-1.2cm) phenocrysts are characteristic of the Pangrango basalts. Clinopyroxene phenocrysts of slightly smaller dimensions are featured in the volcanic products of Gegerbentang. Several clinopyroxene phenocrysts of the Young Gede Other Vent group contain anhedral glass inclusions, similar to those seen in plagioclase phenocrysts of the same group.

Most of the eruptive groups display a fairly restricted range in clinopyroxene composition (Figs. 4a-i). The basaltic andesites of the Young Gede Other Vent group display the greatest within-group variation ($\text{En}_{38-45}\text{Wo}_{38-45}\text{Fs}_{12-20}$, Fig. 4c) and contrast with the highly restricted range in plagioclase composition observed in this group (Fig. 3b). The Pangrango basalts do not possess the most Ca-rich or Fe-poor clinopyroxene compositions, as might be expected in the least evolved (lowest SiO_2) rocks analysed from GVC (Fig. 4f). Pigeonite ($\text{En}_{55}\text{Wo}_{25}\text{Fs}_{20}$) was present in a 4 mm glomerocryst/cumulate xenolith in an Older Quaternary Volcanic group lava (Fig. 4i).

Orthopyroxene

Orthopyroxene phenocrysts are less abundant than clinopyroxene in GVC rocks, and are generally smaller in size. They are subhedral to euhedral, except when mantled by

clinopyroxene, where they are typically anhedral to subhedral. Mantling of orthopyroxene is commonly observed in GVC rocks, especially in some of the basaltic andesites and all of the andesites of the Young Gede Kawah Ratu group. No obvious correlation is observed between the degree and type of plagioclase compositional zoning (and the magnitude of plagioclase core composition variability) and the presence or absence of mantled orthopyroxene (Fig. 3d-f). For example, samples with normally-zoned plagioclase showing only a small difference in An mol% between core to rim (YGKR basaltic andesite, Fig 3e) and samples characterised by significant reversely-zoned plagioclase (Older Quaternary andesite, Fig 3f) both contain orthopyroxene mantled by clinopyroxene.

There is little distinction between orthopyroxene compositions in the basaltic andesites and andesites within most eruptive series. Orthopyroxene enclosed within clinopyroxene in the basaltic andesites of the Young Gede Kawah Ratu and Other Vents groups (Figs. 4a and c) lie among the higher Mg orthopyroxene compositions (En_{68} and En_{70} respectively) of both groups (En_{62-69} and En_{64-71}). Orthopyroxene mantled by clinopyroxene in the basaltic andesites of Pangrango possess identical compositions to those not shrouded by clinopyroxene (Fig. 4g). Orthopyroxene compositions in the Old Gede group (Figs. 4d and e) are comparable to those measured in similarly evolved rocks of Young Gede (both groups).

Olivine

Olivine displays a limited presence in GVC volcanic rocks, restricted to a small number of basalts and basaltic andesites. The anhedral and occasionally embayed olivine phenocrysts are typically smaller than pyroxene and plagioclase phenocrysts within the same samples from the Young Gede Other Vents group. In one sample from Old Gede (G07) olivine is the dominant ferromagnesian phase (Supplementary Table 1) and occurs as large subhedral crystals. In other Old Gede samples olivine phenocrysts are small, anhedral and co-exist with orthopyroxene. Olivine is a major component of the ferromagnesian mineral assemblage in basalts from Pangrango, constituting ~8-12 % of the modal volume. Most crystals are small, commonly with rounded edges, and sometimes occur as inclusions within clinopyroxene. Olivine is only observed in one sample from Gegerbentang, characterised by small anhedral phenocrysts, some showing evidence of resorption.

Olivine compositions are displayed in Fig. 5. Forsterite (Fo) contents of olivines in basaltic andesites of the Young Gede Other Vent group (Fo_{70-72}) are higher than Fo contents in any other GVC group, consistent with the high (most primitive) An contents of plagioclase

phenocrysts (Fig. 3b) of this group. Fo contents of the Pangrango basalts are less magnesium-rich than those in the more evolved rocks of Young Gede.

Fe-Ti oxide

Fe-Ti oxide (titanomagnetite) occurs as phenocrysts, inclusions within ferromagnesian minerals (dominantly clinopyroxene) and as a groundmass phase in most GVC rocks. Titanomagnetite is typically subhedral and constitutes a small percentage of the modal rock volume (~1-3%). Subhedral titanomagnetite phenocrysts are relatively more abundant in the Older Quaternary Volcanic group compared with the majority of GVC rocks (Supplementary Table 1) and have higher than average Ti contents. Relatively high Ti contents are also observed in titanomagnetite phenocrysts in Pangrango lavas (Supplementary Table 6).

Xenoliths

Xenoliths are generally uncommon in GVC rocks. Angular clasts of igneous material ~1mm to 2cm in size are observed within the Young Gede Other Vents group, particularly within juvenile scoria of pyroclastic flow deposits (e.g. G51, G01A). The most abundant type consists of large plagioclase and orthopyroxene phenocrysts, within a fine- to medium-grained groundmass of plagioclase, orthopyroxene and oxide. The holocrystalline clasts, display sharp contacts with the host rock and can be removed relatively easily from the host matrix.

A different type of igneous xenolith, dominated by tabular plagioclase (with melt-inclusions), amphibole and elongate pyroxene was found in G18 (Old Gede). The amphibole is heavily altered, especially at crystal edges where a thick rim of opaque oxide has formed. The contact between the host and the (0.5 x 0.8cm) xenolith is irregular and slightly diffuse.

A cumulate xenolith was found within Pangrango sample G16. The oval-shaped cumulate is ~0.5cm in diameter and composed of relatively large, generally interlocking plagioclase and pyroxene (orthopyroxene and minor clinopyroxene) crystals, with minor interstitial pyroxene. There is no obvious reaction rim at the contact between the cumulate xenolith and the host lava.

Estimation of pre-eruptive temperature and pressure conditions

Pre-eruptive crystallisation temperatures and pressures were estimated using the two-pyroxene approach detailed in Putirka (2008). A summary of the results and calculation conditions are given in Table 1. Magmatic temperatures were calculated according to the

method of Brey and Köhler (1990) and Equation 36 of Putrika (2008). A significant number of pyroxene pairs for many individual samples did not give acceptable equilibrium values ($K_D(\text{Fe-Mg})^{(\text{cpx-opx})} = 1.09 \pm 0.14$) and therefore these results were excluded. An indication of the percentage of ‘in equilibrium’ two-pyroxene combinations of each sample is given in Table 1. For three samples (G23, G51 and G49) none of the pyroxene pairs gave acceptable $K_D(\text{Fe-Mg})^{(\text{cpx-opx})}$ values. This may indicate the incorporation of antecrysts or xenocrysts by the magma or operation of magma mixing processes in these samples. G23 and G49 do in fact display textural disequilibrium features (orthopyroxene mantled by clinopyroxene, Table 1) and G51 displays evidence of magma mingling (Fig. 6). For ‘in equilibrium’ pyroxene pairs, temperatures lie between 891-1014°C (Brey and Köhler, 1990) and 962-1046°C (Equation 36, Putrika, 2008). Two-pyroxene crystallisation pressures were calculated using Equation 39 of Putrika (2008) and gave pressures between 3.4-6.5 kbar, equating to depths below the volcano of ~13-24 km. There are no significant differences in pre-eruptive pressure conditions between geographic groups. However, the most recent eruptives (Young Gede Kawah Ratu) give the widest range in crystallisation depth (~10km).

Magma mingling

Several juvenile scoria samples from pyroclastic flow deposit units of Young Gede (Kawah Ratu and Other Vents) and Old Gede show evidence for the mingling of distinct magmas. The vesicular juvenile scoria is composed of dark grey/black material with irregularly shaped lenses or bands of lighter, pale-grey material. The majority of juvenile scoria from Young Gede are composed of the dark component (Fig. 6a, G36B & G51), while the samples from Old Gede are variably banded with more equal shares of both light and dark layers (Fig. 6c, G13). The dark bands contain phenocrysts of sub- to euhedral plagioclase, clinopyroxene and titanomagnetite and anhedral to subhedral olivine. The lighter layers contain the same mineral assemblage but with orthopyroxene substituted for olivine. Both layers display porphyritic textures (Fig. 6e) and oscillatory zoning and sieve textures in plagioclase phenocrysts. The contact between the two layers is always irregular in detail (Fig. 6e) and ranges from sharp to diffuse, indicating that mixing may have occurred in some samples. The Young Gede juvenile scoria (G36B and G51) possess small, angular xenolith clasts (described above), which display sharp contacts with the host rock.

Compositions of plagioclase and pyroxene phenocrysts in the light and dark layers of sample G51 are plotted in Fig. 6b. Anorthite contents of plagioclase in the dark layer are high and restricted between An_{80-90} . Plagioclase compositions in the light layer of G51 overlap

1 with those in the dark layer in the core (An_{80-90}) but mid and rim sections extend to much
2 lower An contents ($\sim An_{45}$). Clinopyroxene compositions in the light layer of G51 (Fig. 6b)
3 are relatively Fe-rich compared to those measured in the dark layer with the exception of one
4 phenocryst, which plots between the light layer data points. Plagioclase core compositions in
5 G11 (a dark juvenile scoria sample from the same locality as G13) display high (An_{80}) and
6 low (An_{60}) An core contents, with comparably high and low An content in the respective rims
7 (Fig. 6d).

9 **Major element data**

10 Major element data are given in Table 2 and presented in Fig. 7. GVC rocks possess
11 intermediate silica contents ($\sim 51-63$ wt %). Low MgO contents in the basalts ($\sim 4-5$ wt %)
12 suggest that these samples are fractionated and do not represent primary basalts. Major
13 element trends are similar for most of the Gede Complex groups (Figs. 7a-h); negative
14 correlations against silica are displayed for Fe_2O_3 , MgO, CaO and TiO_2 , and positive
15 correlations are generally observed for K_2O and Na_2O . The data show considerable scatter for
16 Al_2O_3 and P_2O_5 versus SiO_2 . Volcanic rocks of Young Gede (both groups) display the
17 greatest range in silica content (52-62 wt %). The Young Gede Other Vents group cluster at
18 ~ 55 wt % SiO_2 and display relatively poor correlations of major elements with SiO_2 . The
19 Pangrango lavas are among the least evolved samples collected from the complex and
20 possess the highest TiO_2 contents, up to ~ 1.2 wt % (Fig. 7g). Eruptives of Gegerbentang
21 cluster towards the lower silica end of the GVC array and possess slighter higher P_2O_5
22 content compared to other GVC rocks of comparable silica content (Fig. 7h).

24 **Trace element geochemistry**

25 Variations of selected trace elements with SiO_2 are presented in Fig. 8. GVC rocks display
26 increases with increasing silica of most LILE (e.g. Ba (Fig. 8a), Rb and here including Th and
27 U), LREE (e.g. La, Fig. 8b) and some HFSE (Zr and Hf, not shown). Nb exhibits a very poor
28 positive correlation (Fig. 8d). Elements that behave compatibly in most arc magmas, such as
29 vanadium and nickel display reasonable (Fig. 8e) to poor (Fig. 8c) negative correlations with
30 SiO_2 in GVC rocks. Ni contents are extremely low ($\sim 1-17$ ppm) in GVC rocks and further
31 confirm their highly fractionated character. Y, Yb, Sr, Pb and Eu data display considerable
32 scatter and remain essentially constant over the range in silica content (e.g. Figs. 8f-h). There
33 is little distinction in trace element variations of the separate eruptive groups.

Sr isotope data

Whole-rock Sr isotope data are listed in Table 3 and displayed in Figs. 2, 9a and 10. $^{87}\text{Sr}/^{86}\text{Sr}$ isotope ratios of volcanic rocks from the Gede Volcanic Complex span a fairly wide range (0.704508-0.705540) compared to other Javan volcanoes (e.g. Ijen Volcanic Complex in East Java, Handley et al. 2007). The Older Quaternary samples possess the most primitive Sr isotope ratios, while Pangrango volcanic rocks possess the highest $^{87}\text{Sr}/^{86}\text{Sr}$ ratios of GVC. Sr isotope ratios of rocks from Young and Old Gede and Gegerbentang generally overlap and form a sub-horizontal array between Pangrango and the Older Quaternary volcanic rocks (Fig. 9a). The Young Gede Other Vent samples display a broad range in Sr isotope ratios over a fairly small range (~2%) in silica. Within-group Sr isotope ratios do not display significant correlation with indices of differentiation; however the complex as a whole displays a slight negative correlation with SiO_2 (Fig. 9a). Although it is beyond the scope of this paper, it is important to note that based on Ba/La and Zr/Nb ratios versus Sr isotope data (Figs. 2a and b), the two oldest volcanic groups, Gegerbentang and the Older Quaternary Volcanics are derived from a magma source of different geochemical composition to the other volcanic groups of GVC.

Oxygen isotope data

Oxygen isotope data are listed in Table 4 and displayed in Figs. 9b and 10. Mineral separates of olivine, clinopyroxene and plagioclase from GVC lavas possess relatively restricted $\delta^{18}\text{O}$ values ranging from +5.32 to +5.42 ‰ (n = 3), +5.52 to +5.94‰ (n = 12) and +6.07‰ (n = 1), respectively. The majority of the GVC data lie within error (2SD) of $\delta^{18}\text{O}$ values measured in mantle olivine ($+5.18 \pm 0.28\text{‰}$, n = 76) and clinopyroxene ($+5.57 \pm 0.32\text{‰}$, n = 57) (Mattey et al. 1994; Ionov et al. 1994, Fig. 10a). Differences in $\delta^{18}\text{O}$ values between coexisting clinopyroxene and olivine ($\Delta_{\text{cpx-ol}}$) and plagioclase and clinopyroxene ($\Delta_{\text{plag-cpx}}$) at GVC are 0.30-0.44‰ and 0.44‰, respectively, suggesting isotopic equilibrium at typical magmatic temperatures for andesite liquids. (Macpherson and Mattey 1998; Macpherson et al. 1998). $\delta^{18}\text{O}$ values from the GVC are slightly higher than $\delta^{18}\text{O}$ clinopyroxene values reported for Galunggung and Salak (Harmon and Gerbe 1992; Handley et al. 2008a) in West Java and Ijen Volcanic Complex in East Java (Handley et al. 2007, Fig. 10) but lie within the range of both clinopyroxene (+5.18 to +7.04‰) and olivine (+4.92 to +5.59‰) $\delta^{18}\text{O}$ values reported for the Banda arc (Vroon et al. 2001). $\delta^{18}\text{O}$ values do not appear to show significant

distinctions between different eruptive centres (Figs. 9b and 10) and do not correlate with indices of differentiation (Fig. 9b).

Discussion

Differentiation of magma

Fractional crystallisation

The predominance of basaltic andesites, low MgO and extremely low Ni contents in basalts of the GVC indicate that the lavas erupted are significantly fractionated. To quantitatively test whether fractional crystallisation of the mineral assemblage observed in GVC rocks is accountable for the major element variations observed (Fig. 7), least squares modelling was employed. Because GVC includes several large volcanic centres, the aims of modelling are 2 fold: 1) To determine whether fractional crystallisation can explain major element variation within each eruptive series. 2) To establish whether the eruptive series of Gede volcano (Young Gede Kawah Ratu, Young Gede Other Vents and Old Gede) may be genetically related by the process of fractional crystallisation.

Least squares modelling of GVC major element data utilises the XLFRAC programme of Stormer and Nicholls (1978). Summaries of least squares modelling results are given in Table 5. Fractional crystallisation models from the least evolved (lowest SiO₂) to the most evolved (highest SiO₂) rocks within each eruptive group yield good to excellent results, with Σr^2 values less than or equal to 0.1 (models 1-11, Table 5). These models suggest that within-group major element variation can be explained by the fractional crystallisation of plagioclase, clinopyroxene, Fe-Ti oxide, plus olivine or orthopyroxene from the most basic end-members within each eruptive group with a maximum degree of crystallisation of 50% (model 10). However, from the basic to evolved members of the Young Gede Other Vents group models requires the addition of 8.6% plagioclase during fractionation of clinopyroxene, orthopyroxene and oxide.

The second objective of least squares modelling is to see if major element variation between Gede volcano sub-units may be explained through crystal fractionation. Models 12-14 show that excellent Σr^2 values of <0.06 are obtained, especially in models using the most basic Old Gede sample as parent to the most evolved Young Gede Kawah Ratu and Other Centre lavas (models 12 and 13, $\Sigma r^2 = 0.03$). However, both of these models require the addition, rather than removal, of a small percentage of clinopyroxene. Using the mineral phase proportions given by model 10 (Table 5), fractionation curves from the least evolved

(lowest SiO₂) Young Gede Kawah Ratu sample (G23) have been calculated and are plotted on Fig. 7 (FC G23). In most cases, excluding TiO₂ (Fig. 7g), the model curves fit the Young Gede Kawah Ratu and general GVC array well, acknowledging data scatter in Al₂O₃ and P₂O₅ versus SiO₂.

To test the conclusions of least squares analysis and investigate whether the concentrations of trace elements in GVC rocks are controlled by fractional crystallisation of the same mineral assemblage, forward modelling of trace element concentrations was conducted using the Rayleigh fractionation equation: $C_l = C_o F^{(D-1)}$, where C_l and C_o represent the concentration of an element in the daughter and parental liquids respectively, F is the fraction of liquid remaining and D is the bulk distribution coefficient. The results and model parameters are given in Fig. 8. The fractionation curves produced (FC G23) show variable success in fitting the array of the GVC data. The best fits are observed for the incompatible elements Ba and La (e.g. Figs. 8a and b) and Nb (Fig. 8d). Acceptable results are noted for V. However, poor fits are observed for other elements. This is largely a consequence of the scatter in the data in Figs. 8c and f-h.

Several models have proposed that the geochemical diversity exhibited by arc lavas is controlled by crystallisation in the mid- to lower crust and that phenocryst textural complexity is subsequently acquired in the upper crust (e.g. Hildreth and Moorbath 1988; Annen et al. 2006). Based on REE ratios, amphibole fractionation at depth (mid- to lower crust) is thought to exert major control on magmatic differentiation in arc volcanoes and at GVC (Davidson et al. 2007). Mid- to lower crustal crystallisation pressures calculated for GVC pyroxenes (Table 1) and the presence of an amphibole-bearing xenolith in an Old Gede lava (G18) give support for amphibole-involved fractionation at depth beneath the GVC. Recent work by Brophy (2008) suggests that mid- to upper crustal hornblende-bearing basalt fractionation will produce steadily increasing LREE abundances but constant and then decreasing HREE abundances, like those observed for GVC lavas in Figs. 8b and 8h. To investigate whether fractionation of amphibole better explains the major and trace element characteristics of GVC rocks, fractionation trends for amphibole (FC Amph) are plotted in Figs. 7 and 8. Overall, magmatic evolution by amphibole fractionation is no more acceptable for reproducing major (e.g. Figs. 7d, e and g) and trace element trends (Fig. 8) than the fractionating phase assemblage observed in the rocks (FC G23). For some elements, the GVC data lie between fractionation curves for amphibole and the observed mineral assemblage in the rock, suggesting that the data may be explained by a combination of both processes (e.g. Figs. 7a, c and g, and 8f and h).

Magma mixing

Magma mixing is important in the evolution of many arc magmas (e.g. Eichelberger et al. 2000; Tepley et al. 2000) and in magmatic evolution at volcanoes of the Sunda arc (Slamet, Reubi et al., 2003; Batur, Reubi and Nicholls 2004; Krakatau, Mandeville et al. 1996; Merapi, Camus et al. 2000). Mingled scoria in volcanic rocks of Young Gede and Old Gede provide unequivocal evidence for the interaction of distinct magmas at GVC (Fig. 6). The question then arises whether or not magma mixing imparts a recognisable influence or control on element concentrations? Petrographic features in GVC rocks such as reverse zoning, sieve textured and resorbed cores in plagioclase phenocrysts, variation in coexisting plagioclase core compositions, mantling of orthopyroxene by clinopyroxene and juxtaposition of olivine with orthopyroxene indicate that closed-system crystal fractionation may be an over-simplistic model for magmatic evolution at GVC. Furthermore, least squares modelling of major element data required the addition of plagioclase or clinopyroxene in some models (Table 5). However, minor zoning and resorption features in plagioclase are not strict evidence for magma mixing, such textures are likely to result from changes in P , T , and PH_2O (e.g. Pearce and Kolisnik, 1990; Ginibre et al. 2002 and references therein). Similarly, sieve-textured plagioclase are commonly interpreted to be produced by magma mixing but experimental data have shown that these textures can also be produced by decompression or heating (Nelson and Montana 1992; Johannes et al. 1994). In most GVC rocks, the amplitude of An mol% variation observed in: 1) plagioclase cores of the same rock and, 2) reversely zoned plagioclase is small (within 20 mol% An, Fig. 3), obviating the necessity of magma mixing. Mantling of orthopyroxene by clinopyroxene in GVC rocks may result from an increase in temperature due to the influx of more primitive magma, but can also be created by convective self-mixing (Couch et al. 2001). Alternatively, mantled orthopyroxene may be antecrystic and entrained by the magma during transit to the surface. The Mg content of mantled orthopyroxenes in basaltic andesites of Young Gede lie among the highest Mg orthopyroxene compositions observed in the rocks (Figs. 4a and c).

To help assess the extent to which magma mixing can account for the geochemical diversity of the lavas, an example mixing line (MM) is plotted on Figs. 7 and 8, between the least- and most evolved Young Gede Kawah Ratu rocks (G23-G39). Rocks of this group were chosen as they show the greatest textural complexity. For major elements (except TiO_2 and P_2O_5 , Figs. 7g and h) and some trace elements (those showing incompatible behaviour during differentiation) the magma mixing (MM) and fractional crystallisation trends (FC

G23) are extremely similar, and indistinguishable from each other in some cases (Figs. 7f and 8b). The horizontal magma mixing trend produced for Ni versus SiO₂ (Fig. 8c) can account for the constant Ni content observed over a range in SiO₂ (cf. the fractionation trend). However, the mixing line itself does not provide a reasonable fit to the rest of the Kawah Ratu data or GVC data as a whole.

In plots of the form A/B versus 1/B, mixing is controlled by the concentration of the denominator in the ratio. Consequently, plots of this type provide a simple check to see if data are consistent with binary mixing as data should form a linear array (Vogel 1982; Langmuir et al. 1978). La and Nd concentrations increase with differentiation in GVC rocks (e.g. Fig. 8b) and so a plot of La/Nd versus 1/Nd should indicate whether or not the systematic variation with SiO₂ is consistent with mixing. Fig. 11a shows poor linearity within each eruptive group and within the GVC data as a whole and is, therefore, inconsistent with simple mixing processes. The solid lines labelled 1, 2 and 3 in Fig. 11a show several mixing trends between members of the same stratigraphical group (see figure caption for details) to give examples of potential mixing lines. The relatively evolved compositions of both the light and dark components in banded juvenile scoria of Old Gede (57 wt% and 59 wt% SiO₂, respectively) also suggest that simple binary mixing, at least of these components, is an unrealistic model for explaining the geochemical variation observed within this group (mixing line 3, Fig. 11a). Furthermore, distinct plagioclase core compositions (Fig 6) are observed in similar sized phenocrysts within the dark, more basic component (G11) of the mingled rocks, indicating that the parental magma to the basic lava may have experienced mingling and mixing with other magma prior to the clear evidence for magma mingling observed in G13. Fractional crystallisation trends FC23 and FC20 (see figure caption for details) and amphibole fractionation (FC Amph) are also incapable of accounting for the general data array (Fig. 11a). Thus neither fractional crystallisation nor mixing alone is capable of explaining the chemical evolution of GVC magma.

To investigate the relationship between geochemistry and petrological complexity GVC samples are classified according to their petrological features e.g. presence of xenoliths, mantled orthopyroxene, magma mingling and coexistence of olivine and orthopyroxene in Figs. 11b (La/Nd versus 1/Nd) and c (Ni versus SiO₂). Ni versus SiO₂ was chosen for its potential to identify samples with the most evidence for mixing (i.e. similar Ni content over a wide range in SiO₂) from those controlled by fractional crystallisation. Both figures show that there is no obvious link between indicators of petrological complexity/disequilibrium and whole-rock geochemical data in GVC lavas and juvenile scoria.

1 In summary, the scatter in major and trace element data preclude control via simple
2 mixing processes. However, multiple magma mixing and mingling events may play a role in
3 modifying the chemical composition of magma during magmatic evolution. Geochemical
4 evolution most likely reflects a combination of fractional crystallisation (of amphibole at
5 depth and the mineral assemblage observed in the rocks) and magma mixing processes,
6 where multiple fractionation trends and mixing end-members are required.

8 Crustal contamination

9 There is substantial evidence from island arc volcanoes (Thirlwall and Graham 1984;
10 Davidson et al. 1987; Ellam and Harmon 1990; Thirlwall et al. 1996; Macpherson et al. 1998;
11 Handley et al. 2008b) for the contamination of primary magmas by arc crust. Contamination
12 is also thought to be an important process in the western Sunda arc (Gasparon et al. 1994;
13 Gasparon and Varne 1998; Chadwick et al. 2007) and responsible for modifying isotope
14 ratios of lavas at Sangeang Api volcano in the eastern Sunda arc (Turner et al. 2003).

15 The incorporation of crustal material during crustal differentiation may generate
16 correlations of isotope ratios with indices of differentiation (e.g. SiO_2 , Rb) in volcanic rock
17 data (e.g. Davidson et al. 2005). However, this assumes that the contaminant will have an
18 isotopic composition distinct from that of magmas ascending from the mantle. Relatively
19 little is known about the composition of the arc crust in West Java. It is hypothesised that
20 West Java is built upon pre-Tertiary, continental-type basement (Hutchinson 1989; Metcalfe
21 1996; Soeria-Atmadja et al. 1998; Hoffmann-Rothe et al. 2001). Hamilton (1979) suggests
22 that the crust in West Java may consist of relatively immature continental crust, ophiolite
23 slivers and older volcanic rocks. Crustal contamination involving these materials may be
24 difficult to detect. Meta-sedimentary/continental-type crustal xenoliths have not been
25 discovered in any GVC units (only clasts of igneous origin are observed) further highlighting
26 the difficulty of identifying 'crustal' contributions in arc lavas. The relatively wide range in
27 Sr isotope ratios of volcanic rocks from the GVC could be the result of the assimilation of arc
28 crust. However, there are no clear correlations between Sr and O isotope ratios and SiO_2
29 within the individual eruptive groups (Fig. 9). There is a slight correlation in the data set as a
30 whole, with the most evolved samples (Older Quaternary) possessing the most primitive
31 radiogenic isotope compositions and the least evolved rocks (Pangrango) display the least
32 primitive Sr isotopic compositions (Fig. 9a). The weak correlation observed is the reverse
33 trend of that expected by the assimilation of continental-type crust during fractional
34 crystallisation (AFC, DePaolo 1981), which typically generates positive correlations between

$^{87}\text{Sr}/^{86}\text{Sr}$ ratios and SiO_2 , e.g. Lesser Antilles (Davidson 1987). It is similar however, to the trend observed in Alicudi lavas in Italy (Peccerillo et al. 2004) where the most mafic magmas display the most ‘contaminated’ isotope signatures. The authors suggest that the higher temperature and lower viscosity of the basalts enables assimilation of a greater volume of crust (relative to the more evolved magmas). The isotopic variation observed at GVC may also be the result of isotopic heterogeneity of the source. To help address the issue of crustal versus source contamination $\delta^{18}\text{O}$ and $^{87}\text{Sr}/^{86}\text{Sr}$ isotope data can be utilised.

A large contrast exists between the low $\delta^{18}\text{O}$ values of the mantle ($+5.57 \pm 0.32\text{‰}$, Matthey et al. 1994; Ionov et al. 1994) and the generally high and variable $\delta^{18}\text{O}$ values (often $> +10\text{‰}$, Davidson and Harmon 1989) of upper crustal materials, due to low temperature interaction with H_2O in the latter. Therefore, the combination of oxygen and radiogenic isotope ratios (e.g. $^{87}\text{Sr}/^{86}\text{Sr}$) can help diagnose involvement of the crust in magma genesis (James 1981; Davidson et al. 2005). The inset diagram of Fig. 10b shows the different curvatures expected for crustal contamination (mixing crust with basalt during magma evolution) and source contamination (mixing sediment into a mantle source prior to production of primary basalt, Davidson et al. 2005) that result from the significant difference in Sr/O ratios of mantle and mantle-derived basalt. The GVC data are displaced from mantle values towards higher $^{87}\text{Sr}/^{86}\text{Sr}$ isotope ratios, but clinopyroxene $\delta^{18}\text{O}$ values of GVC lavas are relatively homogeneous ($+5.52$ to $+5.94\text{‰}$) and low, lying in the region of mantle values (Fig. 10a). In Fig. 10b the GVC data generally lie along a mixing curve representing contamination of the mantle source by a high $\delta^{18}\text{O}$, high $^{87}\text{Sr}/^{86}\text{Sr}$ component, in this case sediment (see figure caption for end member compositions). It is therefore unlikely that the lavas have been contaminated by young or old continental-type material. Ophiolitic material, i.e. oceanic crust, displays a wide range in oxygen isotope ratios due to interaction between basaltic rocks and seawater over a wide range of temperatures (Muehlenbachs 1986). Therefore, if interaction with oceanic basement had been a significant process at GVC we may predict greater scatter in $\delta^{18}\text{O}$ values than observed. Similarly, a wide range of oxygen isotope ratios may develop in the mafic to intermediate edifices and roots of Sunda arc magmatism that pre-dates GVC.

In summary, mantle-like clinopyroxene $\delta^{18}\text{O}$ values of GVC lavas suggest negligible input of high $\delta^{18}\text{O}$ crustal rocks during differentiation. Most variation in Sr isotope ratios of GVC lavas is therefore proposed to arise from variations in source compositions/components.

1 This conclusion is similar to those reached in studies of other Sunda arc volcanoes (Gerbe et
2 al. 1992; Elburg et al. 2002).

4 Summary and conclusion

5 Whole-rock major and trace element compositions within each eruptive series at GVC are the
6 result of a complex interplay of fractional crystallisation (at variable degrees and depths) and
7 inferred multiple-mixing events. Mid- to heavy-REE data and an amphibole-bearing xenolith
8 provide support for significant magmatic differentiation in the mid- to lower crust via
9 fractional crystallisation involving amphibole. Coexisting pyroxene pairs estimate that
10 fractionation takes place at temperatures of 891-1046°C and pressures of 3.4-6.5 kbar,
11 equivalent to ~13-24km depth beneath the volcanoes. Fractional crystallisation of the mineral
12 assemblage observed in the rocks (plagioclase + clinopyroxene + titanomagnetite ± olivine ±
13 orthopyroxene) can largely account for the geochemical variation observed at GVC and most
14 likely plays a role in modifying the composition (to differing degrees) of each magma batch.
15 Whole-rock geochemical data are inconsistent with simple (binary) magma mixing processes.
16 However, multiple mixing events cannot be excluded and may explain the significant scatter
17 observed in variation diagrams.

18 The degree of petrological complexity in GVC volcanic rocks is highly variable
19 within and between each eruptive group, indicative of complex magmatic histories. No
20 simple correlation is observed between disequilibrium features in GVC rocks, such as the
21 degree and type of plagioclase compositional zoning (and the magnitude of plagioclase core
22 composition variability) and the presence or absence of clinopyroxene overgrowths on
23 orthopyroxene. The relatively small changes in mol% An observed in compositional zoning
24 of plagioclase phenocrysts in GVC rocks may be caused by changes in P , T , and PH_2O in the
25 upper crustal magmatic system rather than changes in melt composition. However, banded
26 juvenile scoria provide strong evidence for the (late-stage) interaction of distinct magmas at
27 Gede volcano (Young and Old Gede groups) and suggest that magma ‘mixing’ may be an
28 important eruption-triggering mechanism. The relationship between petrological and
29 geochemical evidence for mixing is not straightforward at GVC. No obvious link is noted
30 between indicators of petrological complexity/disequilibrium (e.g. presence of xenoliths,
31 mantled orthopyroxene, magma mingling and coexistence of olivine and orthopyroxene) and
32 whole-rock geochemical data. For a greater understanding of textural and chemical
33 relationships in GVC volcanic rocks, and to place better constraints on the importance of

1 mixing processes for magmatic evolution, further study would benefit from high-resolution
2 major- and trace-element mineral profiling, backscattered electron imaging (e.g. Ginibre et al.
3 2002) and fine-scale Sr isotope plagioclase profiling (e.g. Davidson and Tepley 1997).

4 Low, mantle-like clinopyroxene $\delta^{18}\text{O}$ values of GVC lavas suggest negligible input of
5 high $\delta^{18}\text{O}$ crustal materials during magmatic differentiation. Poor correlation of Sr isotope
6 ratios with indices of differentiation of GVC rocks precludes significant assimilation of
7 mature continental-type crust with magma beneath the complex. This contrasts with
8 conclusions reached by Gasparon et al. (1994) who proposed that the upper-crust is the
9 dominant source responsible for the ‘crustal’ geochemical and isotopic signatures observed in
10 western Sunda arc lavas. This implies that the relatively thick (compared to East Java) West
11 Javan arc crust is relatively immature and any deep-seated (shallow contamination is not
12 consistent with O-isotope data) crustal contamination evades detection probably due to the
13 similar geochemical characteristics shared by the crust and ascending magma. These
14 conclusions are consistent with the geochemical characteristics of the crustal contaminant
15 acting in AFC at neighbouring Salak (Handley et al. 2008a). However, this does not truly rule
16 out the possibility that continental-type material constitutes part of the crust beneath all of
17 West Java, just that it is not required to explain the geochemical variation observed in GVC
18 lavas and volcanic rocks of other West Javan arc-front volcanoes. Instead, stable and
19 radiogenic isotopes indicate that ‘crustal’ geochemical and isotopic characteristics arise in
20 GVC rocks as a result of contamination of the mantle source. Mantle wedge contamination is
21 also proposed in studies of other Sunda arc volcanoes (Gerbe et al. 1992; Elburg et al. 2002;
22 Gertisser and Keller 2003; Handley et al. 2007). Based on correlations of trace element ratios
23 with strontium isotopes the magmatic source composition of the older geographical units,
24 Gegerbentang and Older Quaternary, is distinct from the younger eruptives of Pangrango and
25 Gede volcanoes.

26 27 Acknowledgements

28 We thank Akhmad Zaennudin and his colleagues at the Volcanic Survey of Indonesia in
29 Bandung for the invaluable logistical help and guidance in the field. For technical support
30 and analytical assistance our thanks go to: Geoff Nowell, Chris Ottley and Dave Sales at
31 Durham University; Dave Plant at the University of Manchester; Dave Lowry at Royal
32 Holloway University of London; Godfrey Fitton and Dodie James at the University of
33 Edinburgh. The manuscript was significantly improved by the detailed editorial comments of

1 T. Grove and two anonymous reviewers. This project was funded by a Natural Environment
2 Research Council studentship (NER/S/A/2001/06127) and supported by the SE Asia
3 Research Group at Royal Holloway, University of London.

References

- Annen C, Blundy JD, Sparks RSJ (2006) The genesis of intermediate and silicic magmas in deep crustal hot zones. *J Petrol* 47:505-539.
- Bottazzi P, Tiepolo M, Vanucci R, Zanetti A, Brumm R, Foley SF, Oberti R (1999) Distinct site preferences for heavy and light REE in amphibole and the prediction of Amph/LDREE. *Contrib Mineral Petrol* 137:36-45.
- Brey GP, Köhler T (1990) Geothermobarometry in four-phase lherzolites II. New thermobarometers, and practical assessment of existing thermobarometers. *J Petrol* 31:1353-1378.
- Brophy JG (2008) A study of rare earth element (REE)-SiO₂ variations in felsic liquids generated by basalt fractionation and amphibolite melting: a potential test for discriminating between the two different processes. *Contrib Mineral Petrol* 156:337-357.
- Camus G, Gourgaud A, Mossand-Berthommier P, Vincent PM (2000) Merapi (Central Java, Indonesia): an outline of the structural and magmatological evolution with a special emphasis to the major pyroclastic events. *J Volcanol Geotherm Res* 100:139-163.
- Chadwick JP, Troll VR, Ginibre C, Morgan D, Gertisser R, Waight TE, Davidson JP (2007) Carbonate Assimilation at Merapi Volcano, Java, Indonesia: Insights from Crystal Isotope Stratigraphy. *J Petrol* 48:1793-1812.
- Couch S, Sparks RSJ, Carroll MR (2001) Mineral disequilibrium in lavas explained by convective self-mixing in open magma chambers. *Nature* 411:1037-1039.
- Davidson JP (1987) Crustal contamination versus subduction zone enrichment: Examples from the Lesser Antilles and implications for mantle source compositions of island arc volcanic rocks. *Geochim Cosmochim Acta* 51:2185-2198.
- Davidson JP, Dungan MA, Ferguson KM, Colucci MT (1987) Crust-magma interactions and the evolution of arc magmas: The San Pedro-Pellado volcanic complex, southern Chilean Andes. *Geology* 15:443-446.
- Davidson JP, Hora JM, Garrison JM, Dungan MA (2005) Crustal forensics in arc magmas. *J Volcanol Geotherm Res* 140:157-170.

- Davidson JP, Harmon RS (1989) Oxygen isotope constraints on the petrogenesis of volcanic arc magmas from Martinique, Lesser Antilles. *Earth Planet Sci Lett* 95:255-270.
- Davidson JP, Tepley III FJ (1997) Recharge in volcanic systems; evidence from isotope profiles of phenocrysts. *Science* 275:826-829.
- Davidson J, Turner S, Handley H, Macpherson C, Dosseto A (2007) Amphibole “sponge” in arc crust? *Geology* 35:787-790.
- DePaolo DJ (1981) Trace element and isotopic effects of combined wallrock assimilation and fractional crystallization. *Earth Planet Sci Lett* 53:189-202.
- Dowall DP, Nowell GM, Pearson DG (2003) Chemical pre-concentration procedures for high-precision analysis of Hf-Nd-Sr isotopes in geological materials by plasma ionisation multi-collector mass spectrometry (PIMMS) techniques. *Plasma Source Mass Spectrometry*. Spec Pub Royal Society of Chemistry 321-337.
- Edwards CMH (1990) Petrogenesis of tholeiitic, calc-alkaline and alkaline volcanic rocks, Sunda arc, Indonesia. PhD Thesis, Royal Holloway, University of London.
- Effendi AC, Kusnama, Hermanto B (1998) Geological map of the Bogor quadrangle, Java. Volcanological Survey of Indonesia.
- Eichelberger JC, Chertkoff DG, Dreher ST, Nye CJ (2000) Magmas in collision: Rethinking chemical zonation in silicic magmas. *Geology* 28:603-606.
- Elburg M, van Bergen M, Hoogewerff J, Foden J, Vroon P, Zulkarnain I, Nasution A (2002) Geochemical trends across an arc-continent collision zone: magma sources and slab-wedge transfer processes below the Pantar Strait volcanoes, Indonesia. *Geochim Cosmochim Acta* 66:2771-2789.
- Ellam RM, Harmon RS (1990) Oxygen isotope constraints on the crustal contribution to the subduction-related magmatism of the Aeolian Islands, southern Italy. *J Volcanol Geotherm Res* 44:105-122.
- Ewart A (1982) The mineralogy and petrology of Tertiary-Recent orogenic volcanic rocks: with special reference to the andesitic-basaltic compositional range. In: Thorpe RS (Ed.) *Andesites: Orogenic Andesites and Related Rocks*. Wiley, Chichester 525-548.
- Foden JD (1983) The petrology of the calcalkaline lavas of Rindjani volcano, East Sunda arc: a model for island arc petrogenesis. *J Petrol.* 24:98-130.
- Gamble JA, Wood CP, Price RC, Smith IEM, Stewart RB, Waight T (1999) A fifty year perspective of magmatic evolution on Ruapehu Volcano, New Zealand: verification of open system behaviour in an arc volcano. *Earth Planet Sci Lett* 170:301-314.

- 1 Gasparon M, Hilton DR, Varne R (1994) Crustal contamination processes traced by helium
2 isotopes: Examples from the Sunda arc, Indonesia. *Earth Planet Sci Lett* 126:15-22.
- 3 Gasparon M, Varne R (1998) Crustal assimilation versus subducted sediment input in west
4 Sunda arc volcanics: an evaluation. *Mineral Petrol* 64:89-117.
- 5 Gerbe M-C, Gouraud A, Sigmarsson O, Harmon RS, Joron J-L, Provost A (1992)
6 Mineralogical and geochemical evolution of the 1982-1983 Galunggung eruption
7 (Indonesia). *Bull Volcanol* 54:284-298.
- 8 Gertisser R, Keller J (2003) Trace element and Sr, Nd, Pb and O isotope variations in
9 medium-K and high-K volcanic rocks from Merapi Volcano, Central Java, Indonesia:
10 evidence for the involvement of subducted sediments in Sunda Arc magma genesis. *J*
11 *Petrol* 44:457-489.
- 12 Ginibre C, Wörner G, Kronz A (2002) Minor- and trace-element zoning in plagioclase:
13 implications for magma chamber processes at Parinacota volcano, northern Chile.
14 *Contrib Mineral Petrol* 143:300-315.
- 15 Hamilton WB (1979) Tectonics of the Indonesian region. U.S. Geological Survey
16 Professional Paper reprinted with corrections, 1981 and 1985 1078:345.
- 17 Handley HK, Davidson JP, Macpherson CG (2008a) Untangling differentiation in arc lavas:
18 constraints from unusual minor and trace element variations at Salak Volcano,
19 Indonesia. *Chem Geol* 255:360-376
- 20 Handley HK, Macpherson CG, Davidson JP, Berlo K, Lowry D (2007) Constraining fluid
21 and sediment contributions to subduction-related magmatism in Indonesia: Ijen
22 Volcanic Complex, Indonesia. *J Petrol* 48:1155-1183.
- 23 Handley HK, Turner S, Smith IEM, Stewart RB, Cronin SJ (2008b) Rapid timescales of
24 differentiation and evidence for crustal contamination at intra-oceanic arcs:
25 Geochemical and U-Th-Ra-Sr-Nd isotopic constraints from Lopevi Volcano, Vanuatu,
26 SW Pacific. *Earth Planet Sci Lett* 273:184-194.
- 27 Harmon RS, Gerbe MC (1992) The 1982-83 eruption at Galunggung volcano, Java
28 (Indonesia): oxygen isotope geochemistry of a zoned magma chamber. *J Petrol* 33:585-
29 609.
- 30 Hildreth W, Moorbath S (1988) Crustal contributions to arc magmatism in the Andes of
31 Central Chile. *Contrib Mineral Petrol* 98:455-489.
- 32 Hoffmann-Rothe A, Ritter O, Haak V (2001) Magnetotelluric and geomagnetic modelling
33 reveals zones of very high electrical conductivity in the upper crust of Central Java.
34 *Physics of the Earth and Planetary Interiors* 124:131-151.

- 1 Hutchinson CS (1989) Geological evolution of South-east Asia. Oxford Monographs on
2 Geology and Geophysics 13:368pp.
- 3 Ionov DA, Harmon RS, France-Lanord C, Greenwood B, Ashchepkov IV (1994) Oxygen
4 isotope composition of garnet and spinel peridotites in the continental mantle: Evidence
5 from the Vitim xenolith suite, southern Siberia. *Geochim Cosmochim Acta* 58:1463-
6 1470.
- 7 James DE (1981) The combined use of oxygen and radiogenic isotopes as indicators of
8 crustal contamination. *Ann Rev Earth Planet Sci* 9:311-344.
- 9 Johannes W, Koepke J, Behrens H (1994) Partial melting reactions of plagioclases and
10 plagioclase-bearing systems. In Parson I (ed) *Feldspars and their reactions*. Kluwer,
11 Dordrecht, pp 161-194.
- 12 Langmuir CH, Voche RD, Hanson GN, Hart SR (1978) A general mixing equation with
13 applications to Icelandic basalts. *Earth Planet Sci Lett* 37:380-392.
- 14 Macpherson CG, Gamble JA, Matthey DP (1998) Oxygen isotope geochemistry of lavas from
15 an oceanic to continental arc transition, Kermadec-Hikurangi margin, SW Pacific. *Earth*
16 *Planet Sci Lett* 160:609-621.
- 17 Macpherson CG, Matthey DP (1998). Oxygen isotope variations in Lau Basin lavas. *Chem*
18 *Geol* 144:177-194.
- 19 Mandeville CW, Carey S, Sigurdsson H (1996) Magma mixing, fractional crystallisation and
20 volatile degassing during the 1883 eruption of Krakatau volcano, Indonesia. *J Volcanol*
21 *Geotherm Res* 74:243-274.
- 22 Matthey D, Lowry D, Macpherson C (1994) Oxygen isotope composition of mantle peridotite.
23 *Earth Planet Sci Lett* 128:231-241.
- 24 Metcalfe I (1996) Pre-Cretaceous evolution of SE Asian terranes. *Geol Soc Spec Pub* 106:97-
25 122.
- 26 Muehlenbachs K (1986) Alteration of the oceanic crust and the ^{18}O history of seawater.
27 *Reviews in Mineralogy* 16:425-444.
- 28 Nelson ST, Montana A (1992) Sieve-textured plagioclase in volcanic rocks produced by
29 rapid decompression. *Am Mineral* 77:1242-1249.
- 30 Pearce TH, Kolisnik AM (1990). Observations of plagioclase zoning using interference
31 imaging. *Earth-Sci Rev* 29:9-26.
- 32 Peccerillo A, Dallai L, Frezzotti ML, Kempton PD (2004) Sr-Nd-Pb-O isotopic evidence for
33 decreasing crustal contamination with ongoing magma evolution at Alicudi volcano

(Aeolian arc, Italy): implications for style of magma-crust interaction and for mantle source compositions. *Lithos* 78:217-233.

Putirka K (2008). Thermometers and Barometers for Volcanic Systems. In: Putirka K, Tepley F (Eds.), *Minerals, Inclusions and Volcanic Processes, Reviews in Mineralogy and Geochemistry*, Mineralogical Soc. Am. 69:61-120.

Reubi O, Nicholls IA (2004) Magmatic evolution at Batur volcanic field, Bali, Indonesia: petrological evidence for polybaric fractional crystallisation and implications for caldera-forming eruptions. *J Volcanol Geotherm Res* 138:345-369.

Reubi O, Nicholls IA, Kamenetsky VS (2003) Early mixing and mingling in the evolution of basaltic magmas: evidence from phenocryst assemblages, Slamet Volcano, Java, Indonesia. *J Volcanol Geotherm Res* 119:255-274.

Schön JH (2004). Physical properties of rocks: fundamentals and principles of petrophysics. in: Helbig K, Treitel S (eds) 18, Elsevier, UK, 583p.

Sitorus K (1990) Volcanic stratigraphy and geochemistry of the Idjen Caldera Complex, East Java, Indonesia, MSc thesis, University of Wellington, New Zealand.

Situmorang T, Hadisantono RD (1992) Geological map of Gede Volcano, Cianjur, West Java. Volcanic Survey of Indonesia.

Soeria-Atmadja R, Suparka S, Abdullah C, Noeradi D, Sutanto (1998). Magmatism in western Indonesia, the trapping of the Sumba Block and the gateways to the east of Sundaland. *Journal of Asian Earth Sciences* 16:1-12.

Stormer JC Jr, Nicholls J (1978) XLFRAC; a program for the interactive testing of magmatic differentiation models. *Computers & Geosciences* 4:143-159.

Tepley FJ III, Davidson JP, Tilling RI, Arth JG (2000) Magma mixing, recharge and eruption histories recorded in plagioclase phenocrysts from El Chichon, Mexico. *J Petrol* 41:1397-1411.

Thirlwall MF, Graham AM (1984) Evolution of high-Ca, high-Sr C-series basalts from Grenada, Lesser Antilles: the effects of intra-crustal contamination. *J Geol Soc London* 141:427-445.

Thirlwall MF, Graham AM, Arculus RJ, Harmon RS, Macpherson CG (1996) Resolution of the effects of crustal assimilation, sediment subduction, and fluid transport in island arc magmas: Pb-Sr-Nd-O isotope geochemistry of Grenada, Lesser Antilles. *Geochim Cosmochim Acta* 60:4785-4810.

Turner S, Foden J (2001) U, Th and Ra disequilibria, Sr, Nd and Pb isotope and trace element variations in Sunda arc lavas: predominance of a subducted sediment component. *Contrib Mineral Petrol* 142:43-57.

Turner S, Foden J, George R, Evans P, Varne R, Elburg M, Jenner G (2003) Rates and processes of potassic magma evolution beneath Sangeang Api volcano, East Sunda Arc, Indonesia. *J Petrol* 44:491-515.

Vogel TA (1982) Magma mixing in the acidic-basic complex of Ardnamurchan; implications on the evolution of shallow magma chambers. *Contrib Mineral Petrol* 79:411-423.

Vroon PZ, Lowry D, van Bergen MJ, Boyce AJ, Matthey DP (2001) Oxygen isotope systematics of the Banda arc: Low $\delta^{18}\text{O}$ despite involvement of subducted continental material in magma genesis. *Geochim Cosmochim Acta* 65:589-609.

VSI: Volcanic Survey of Indonesia. <http://www.vsi.esdm.go.id/volcanoes/>

Figure Captions

Fig. 1. Topographic sketch map of the Gede Volcanic Complex (GVC) showing the distribution of rock samples and corresponding data symbols used in subsequent figures (see inset for details). Selected rivers are shown by dashed lines. Solid lines with tick marks highlight volcanic craters and escarpments. Gumuruh is the remnant of the Old Gede Crater. Gede represents both Young Gede eruptive groups (Kawah Ratu and Other Vents). Inset diagram shows the location of Gede (large black triangle) in West Java, in relation to major centres of population (grey fill) and other Quaternary volcanoes (small black triangles). The relative stratigraphic age of each volcanic centre is also shown.

Fig. 2. a) Ba/La versus $^{87}\text{Sr}/^{86}\text{Sr}$ and b) Zr/Nb versus $^{87}\text{Sr}/^{86}\text{Sr}$ highlighting heterogeneity in magmatic source composition (arrow labelled SH) for different geographic groups of GVC.

Fig. 3. a-c) Plagioclase analyses of volcanic rocks from the GVC separated by eruptive group (YGKR, Young Gede Kawah Ratu; YGOV, Young Gede Other Vents; OG, Old Gede; PAN, Pangrango; Geg, Gegerbentang; OQ, Older Quaternary volcanics) and rock type. d-f) mol% An differences between plagioclase core and rim (open squares) of similar sized phenocrysts (~500-800 μm in diameter) of selected samples, and mol% An differences in plagioclase core compositions within individual samples (stars). Also shown are samples containing orthopyroxene mantled by clinopyroxene (filled circles).

Fig. 4. Analyses of pyroxene phenocrysts in GVC lavas and juvenile scoria. Dashed lines represent 10% increments.

Fig. 5. Analyses of olivine phenocrysts in basalt from Pangrango and basaltic andesites of Young Gede (Kawah Ratu and Other Vents) and Gegerbentang.

Fig. 6. Details of magma mingling in GVC rocks. a) photograph of juvenile scoria from pyroclastic flow deposits of the Young Gede Other Vents group. b) plagioclase and pyroxene analyses in mingled juvenile scoria sample G51. 'dark' and 'light' correspond to the layer from which they were analysed. c) photograph of juvenile scoria from pyroclastic flow deposits of Old Gede. d) plagioclase core, mid and rim compositions in the dark section of G11. e) micrograph showing detail of the contact between the light and dark layers in mingled juvenile scoria sample G13.

Fig. 7. Major element variation diagrams for GVC rocks. Model fractionation curves (FC) are shown for 100% amphibole fractionation (FC Amph) from GVC basaltic andesite (G23) using the hornblende mineral composition for 8 kbar and 1000 °C of Rapp and Watson (1995), and for fractionation of the mineral assemblage proportions suggested by least squares modelling for model 10 in Table 5: 0.66 Plag, 0.16 Cpx, 0.10 Ol, 0.07 Fe-Ti oxide (FC G23) using mineral data from Supplementary Tables 2-6. Tick marks on fractionation curves indicate the degree of magmatic crystallisation in 10% increments. MM is a magma mixing line between Young Gede Kawah Ratu rocks G23 and G39.

Fig. 8. Selected trace element variations with SiO₂ for GVC rocks. See Fig. 7 for details of model fractionation curves FC Amph and FC G23, and magma mixing line MM. FC G23 mineral partition coefficients are given in Supplementary Table 7. Amphibole partition coefficients are taken from Bottazzi et al. (1999). Tick marks on fractionation curves indicate the degree of magmatic crystallisation in 10% increments.

Fig. 9. Variation of: a) Sr isotope ratios and b) O isotope ratios with SiO₂ for GVC rocks. Arrows labelled SH, AFC and FC indicate the hypothesised data trends related to: heterogeneity in the mantle source (SH), combined assimilation and fractional crystallisation (AFC) and fractional crystallisation (FC). AFC trends can be positive or negative depending

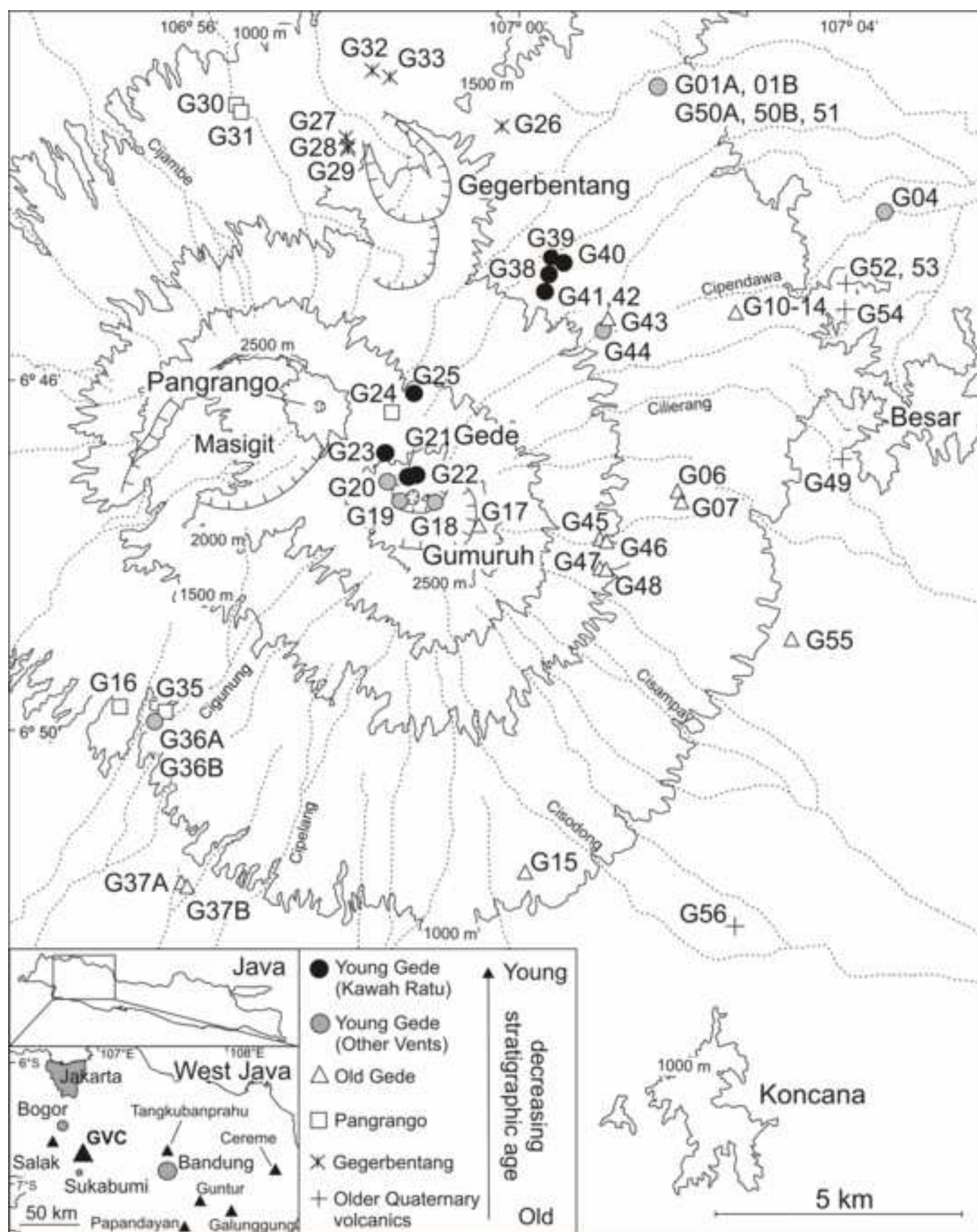
on the Sr isotope ratio of the assimilated material (e.g. continental versus oceanic crust, respectively).

Fig. 10. a) $\delta^{18}\text{O}$ (clinopyroxene) versus $^{87}\text{Sr}/^{86}\text{Sr}$ (whole rock) for GVC lavas showing within-group $\delta^{18}\text{O}$ and $^{87}\text{Sr}/^{86}\text{Sr}$ relationships. Mantle range of clinopyroxene (5.57 ± 0.32 ‰) from Matthey et al. (1994) and Ionov et al. (1994). Java clinopyroxene $\delta^{18}\text{O}$ data: Galunggung (Harmon and Gerbe 1992); Banda arc (Vroon et al. 2001); IVC (Handley et al. 2007) and Salak (Handley et al. 2008a). b) Plot of $\delta^{18}\text{O}$ (clinopyroxene) versus $^{87}\text{Sr}/^{86}\text{Sr}$ (bulk rock) for GVC lavas. A simple mixing curve is plotted between sediment and depleted mantle source to illustrate that GVC lavas are consistent with ‘source contamination’ rather than ‘crustal contamination’. Tick marks indicate the amount of sediment added to the mantle source. Data used in mixing calculation: Bulk sediment Sr = 450 ppm; O = 50.2 wt %, $^{87}\text{Sr}/^{86}\text{Sr} = 0.7156$; $\delta^{18}\text{O} = 18.7$ ‰ (Vroon et al. 2001). Depleted mantle source: Sr = 12.94 ppm; O = 43.8 wt %, $^{87}\text{Sr}/^{86}\text{Sr} = 0.7026$ (Vroon et al. 2001 and references therein); $\delta^{18}\text{O} = 5.57$ ‰ (Matthey et al. 1994; Ionov et al. 1994). Inset diagram shows the expected data trends for ‘crustal’ versus ‘source’ contamination.

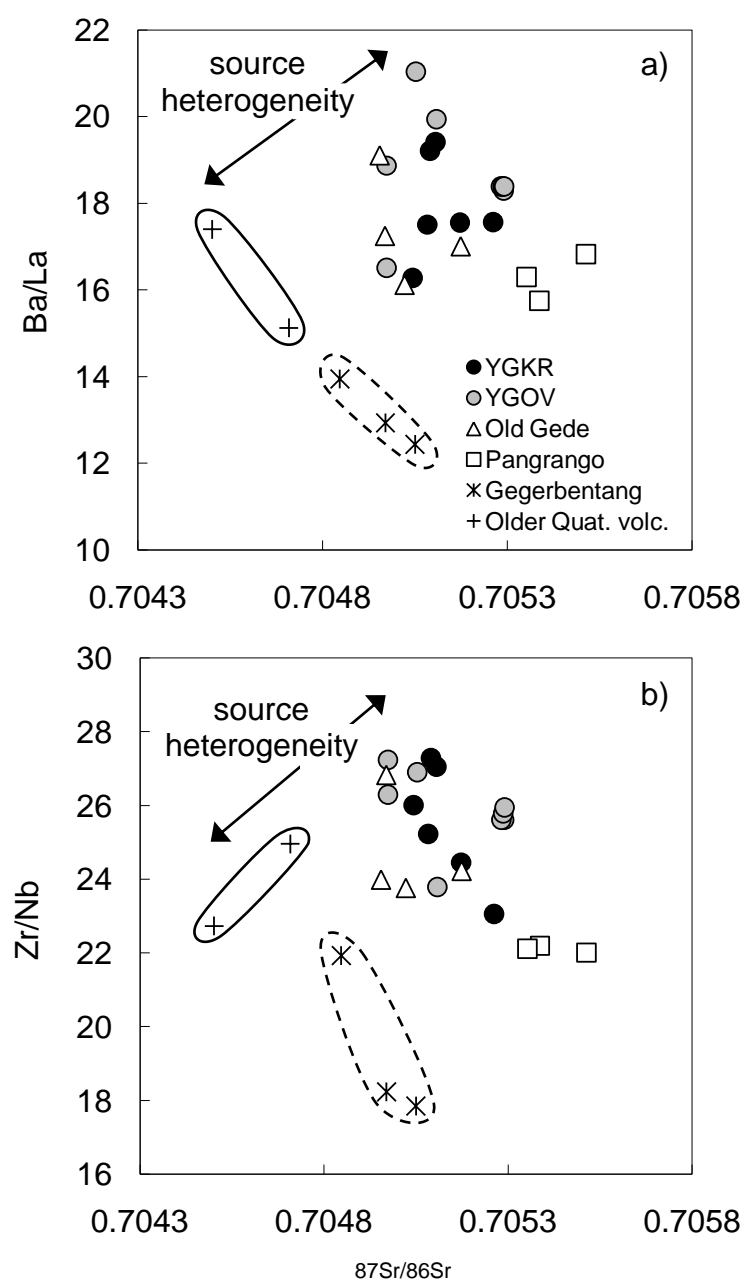
Fig. 11. a) La/Nd versus 1/Nd for GVC rocks classified by eruptive group (symbols as in Fig. 1) showing that the GVC data are not consistent with simple binary mixing or closed-system fractional crystallisation. Model fractionation curves FC Amph and FC G23 as in Figs. 7 and 8. Model fractionation curve from end member G20 (FC G20) uses mineral proportions suggested by least squares modelling for model 7 in Table 5: 0.44 Plag, 0.06 Cpx, 0.34 Ol, 0.15 Fe-Ti oxide and mineral data from G20 (Supplementary Tables 2-6). Solid lines labelled 1, 2 and 3 represent mixing lines between rock samples G23-G39 (Young Gede Kawah Ratu), G20-G18 (Young Gede Other Vents) and G11-G14 (Old Gede), respectively. b) La/Nd versus 1/Nd for GVC rocks with textural information highlighted (symbols as in c). c) Ni versus SiO_2 for GVC rocks with textural information highlighted

Fig. 1

[Click here to download high resolution image](#)



Fig_2
[Click here to download line figure: Fig_2.xls](#)



Fig_3

[Click here to download high resolution image](#)

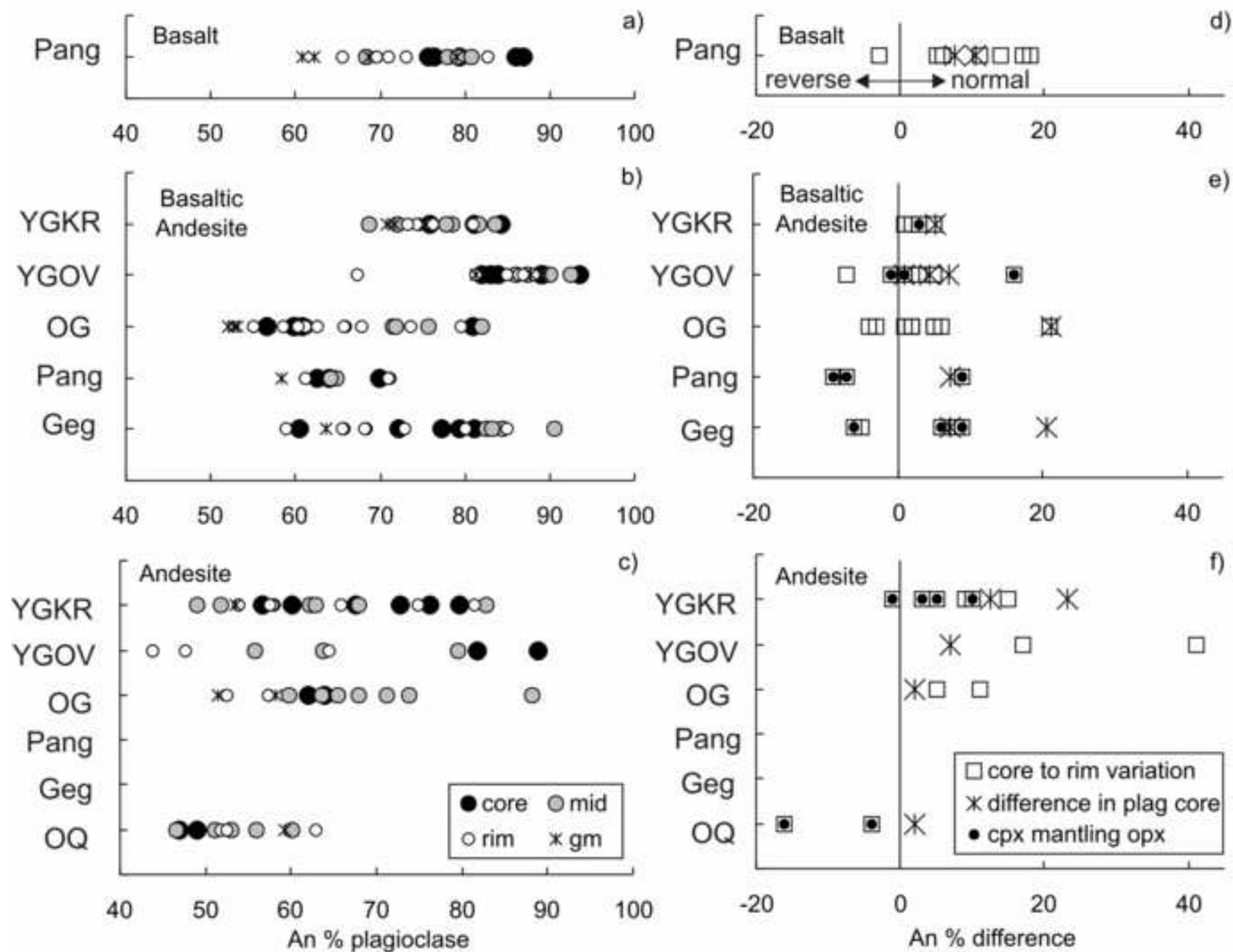


Fig_4

[Click here to download high resolution image](#)

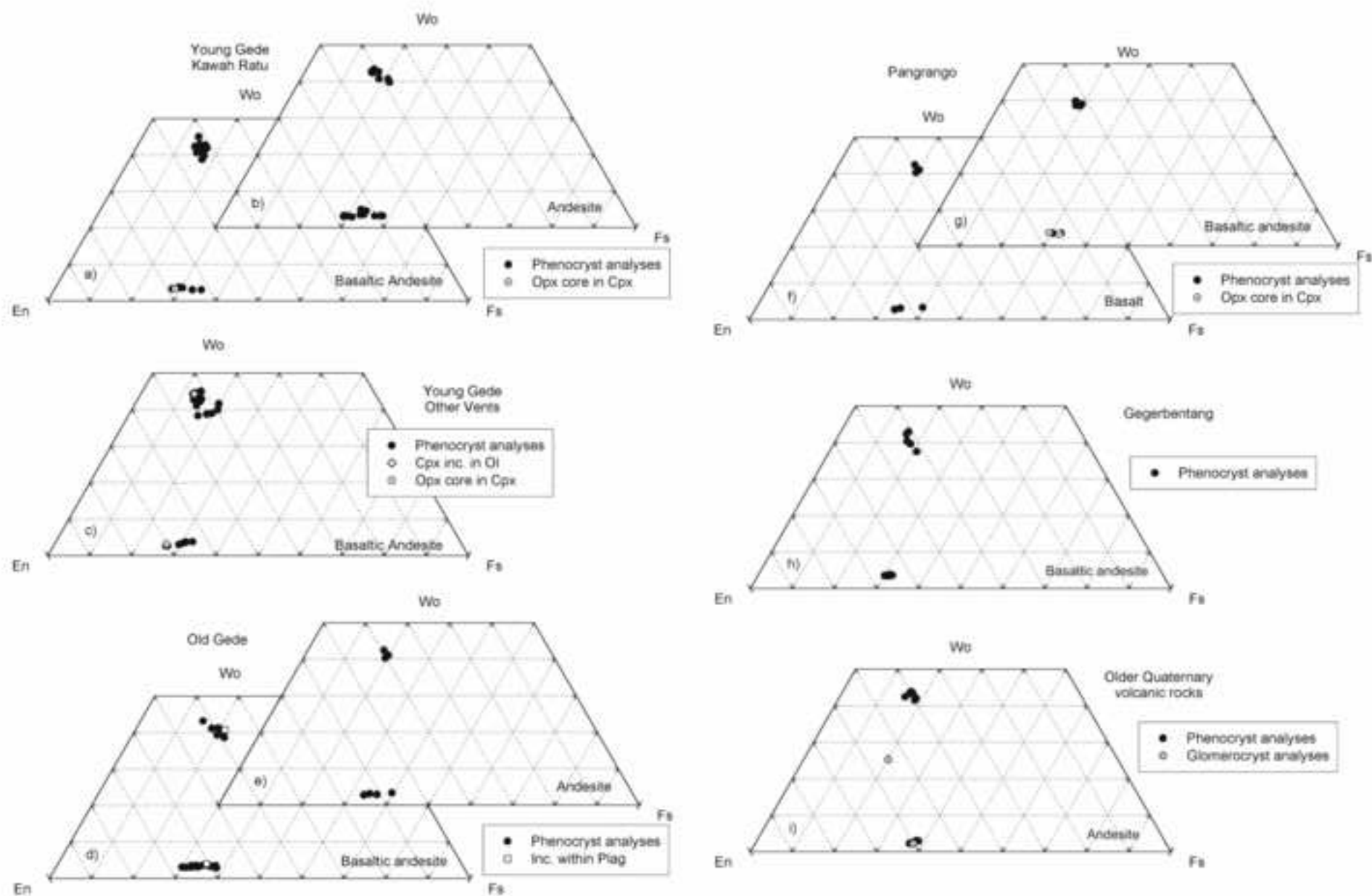


Fig_5
[Click here to download high resolution image](#)

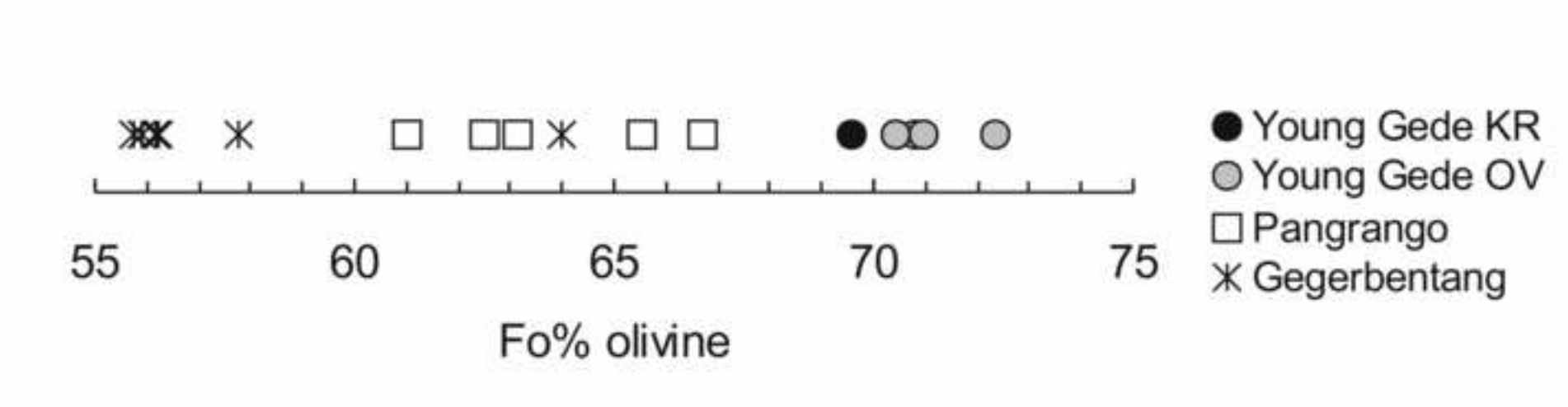
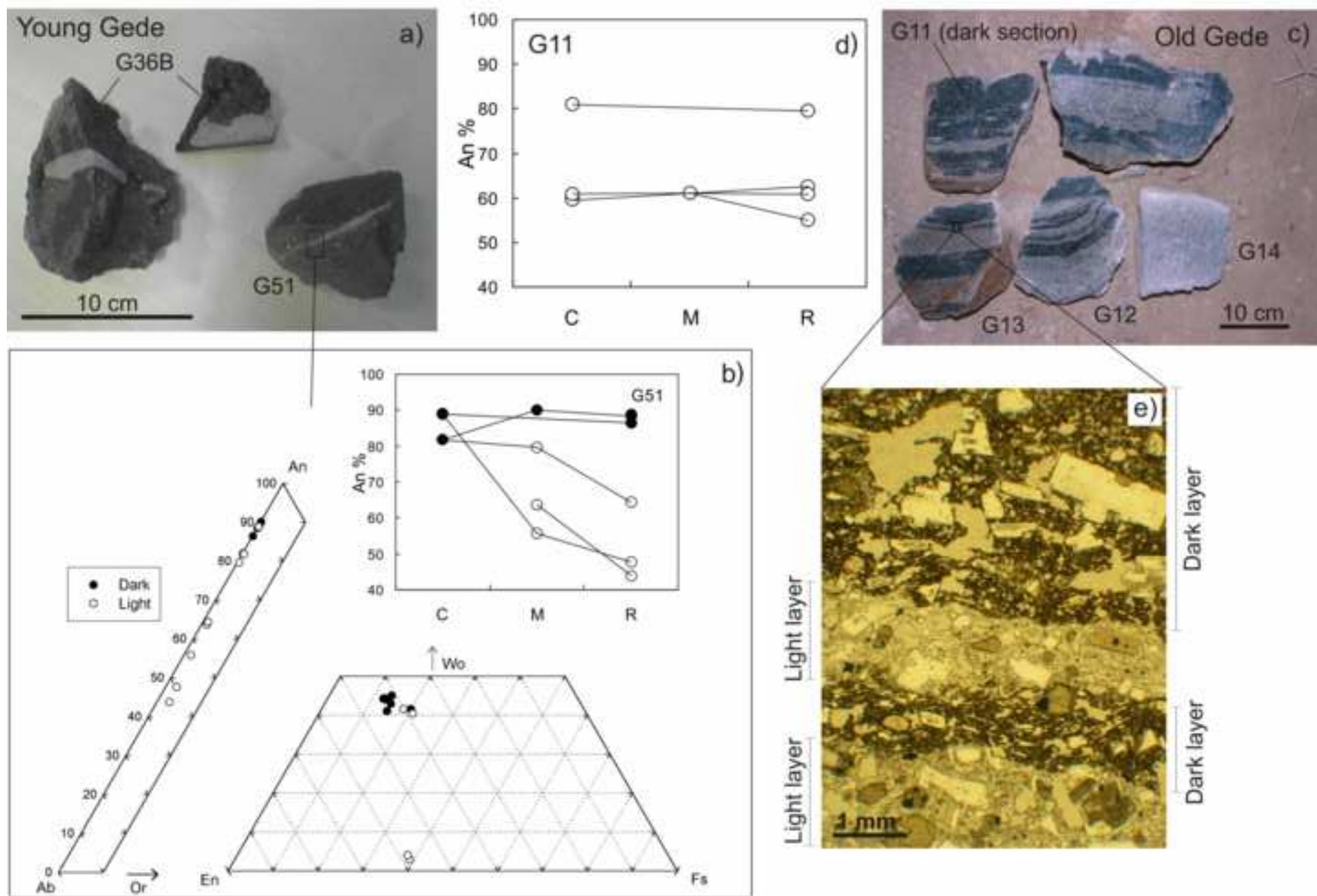


Fig. 6

[Click here to download high resolution image](#)



Fig_7

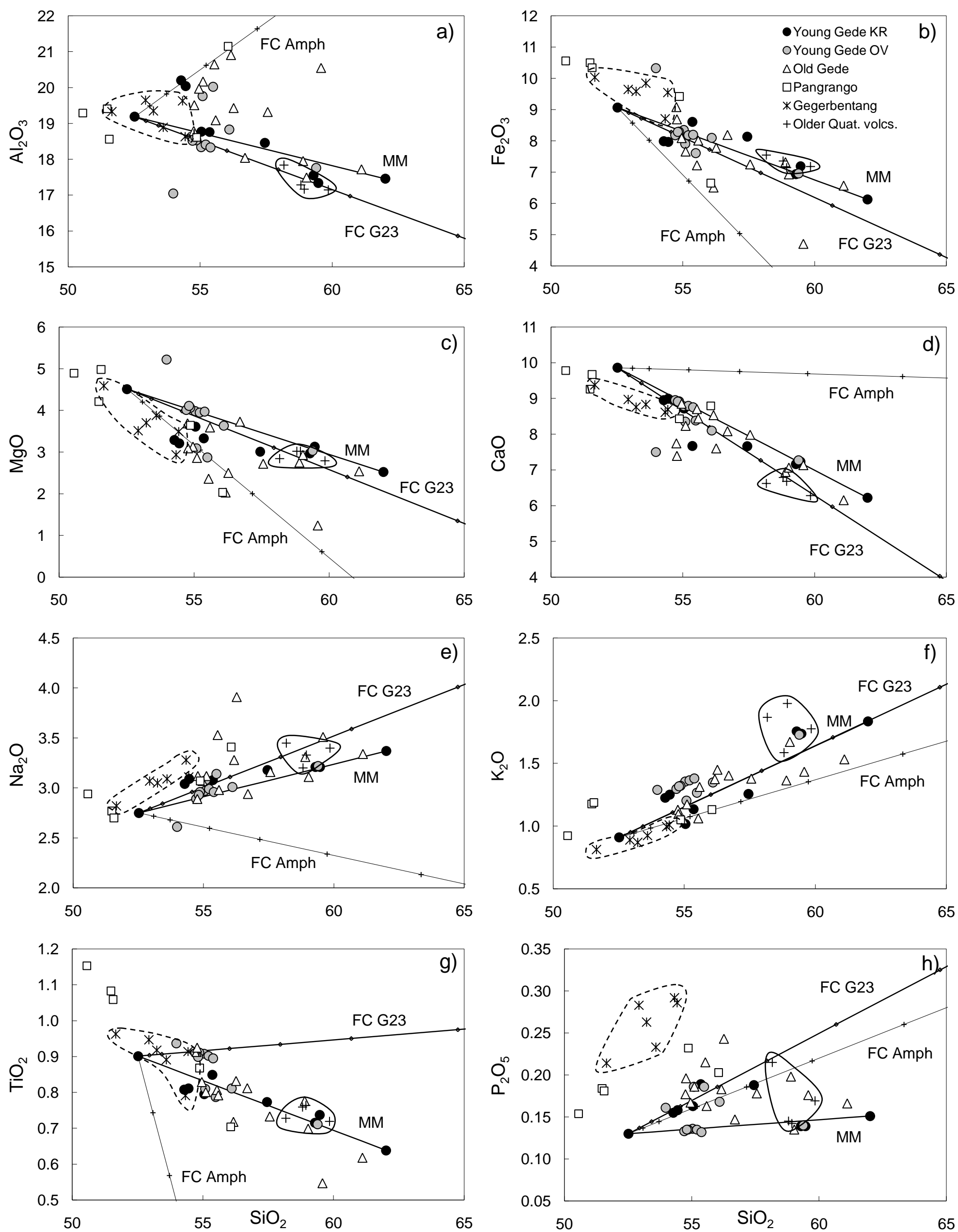
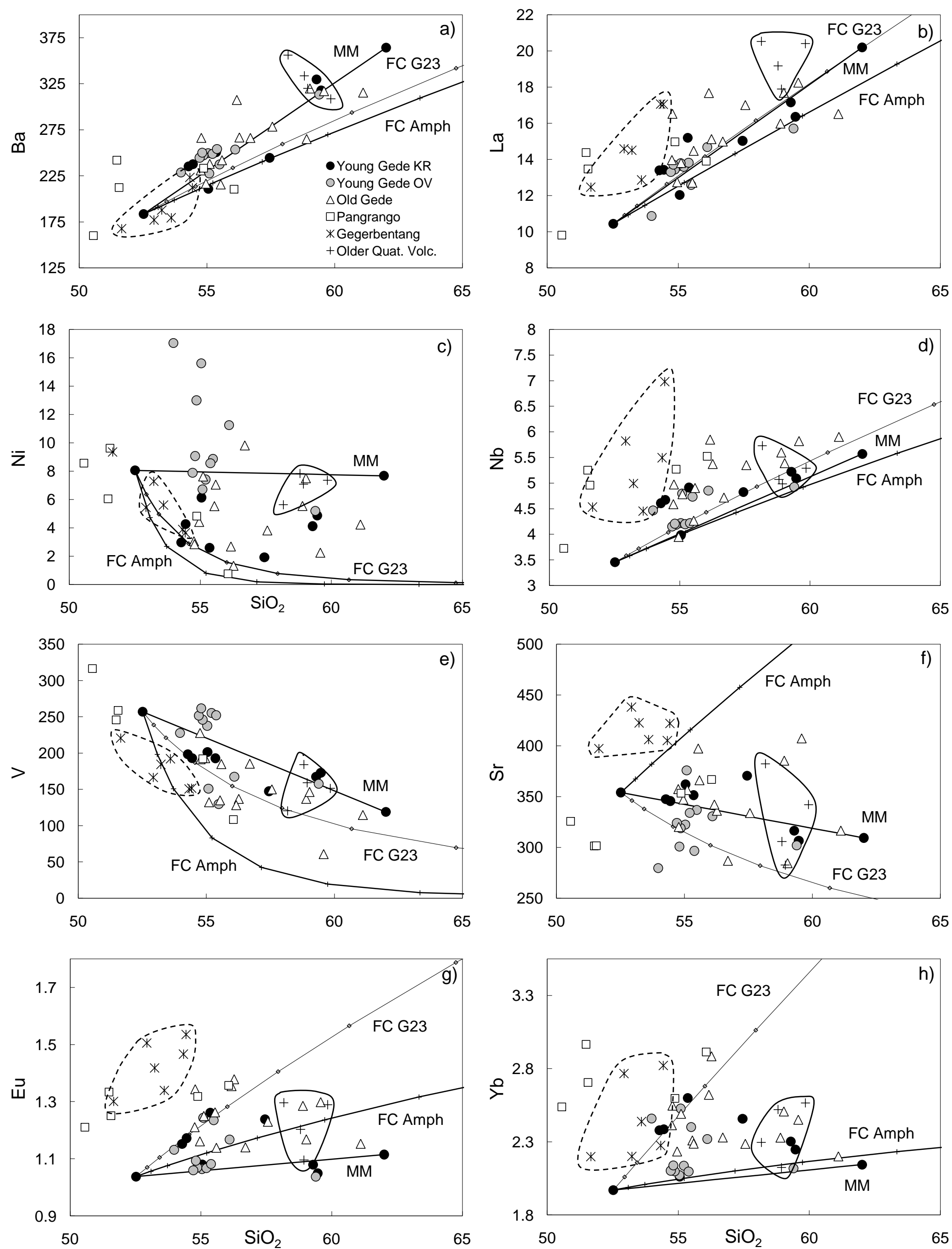
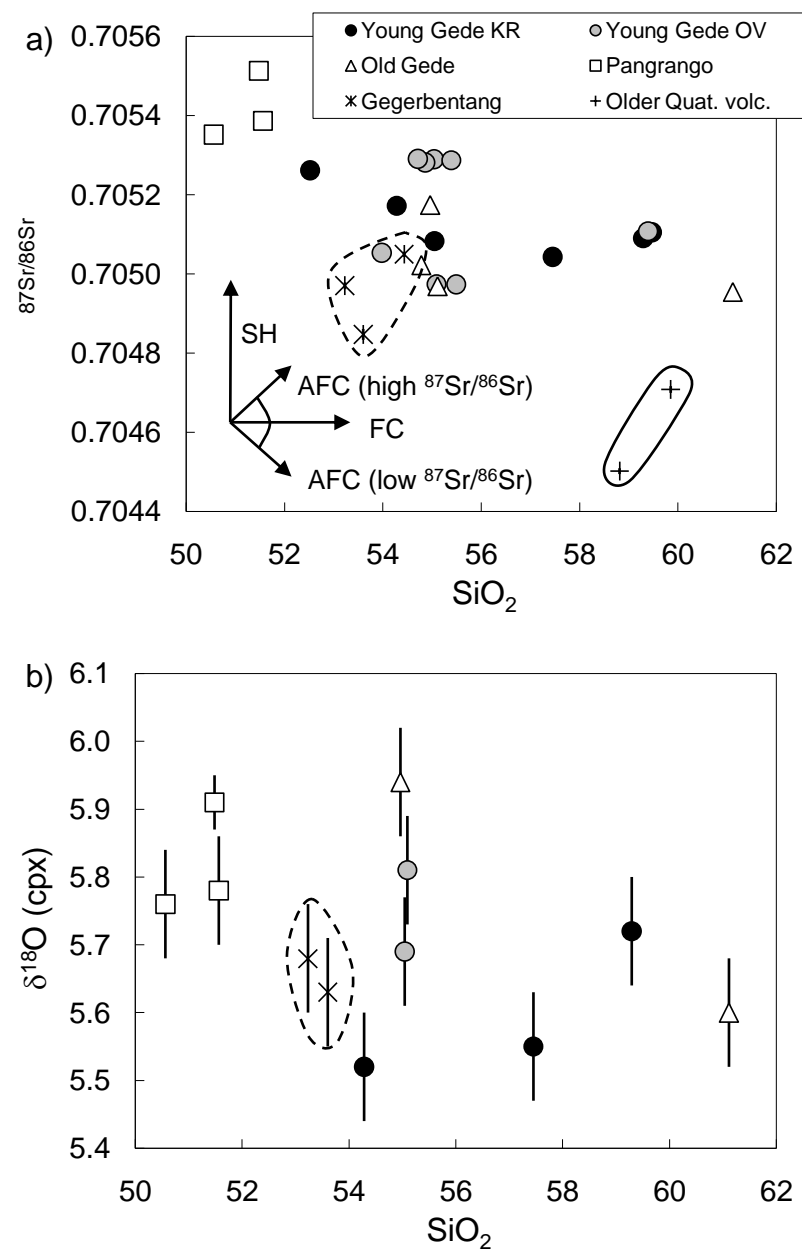
[Click here to download line figure: Fig_7.xls](#)

Fig 8

[Click here to download line figure: Fig_8.xls](#)

Fig_9
[Click here to download line figure: Fig_9.xls](#)



Fig_10

[Click here to download high resolution image](#)

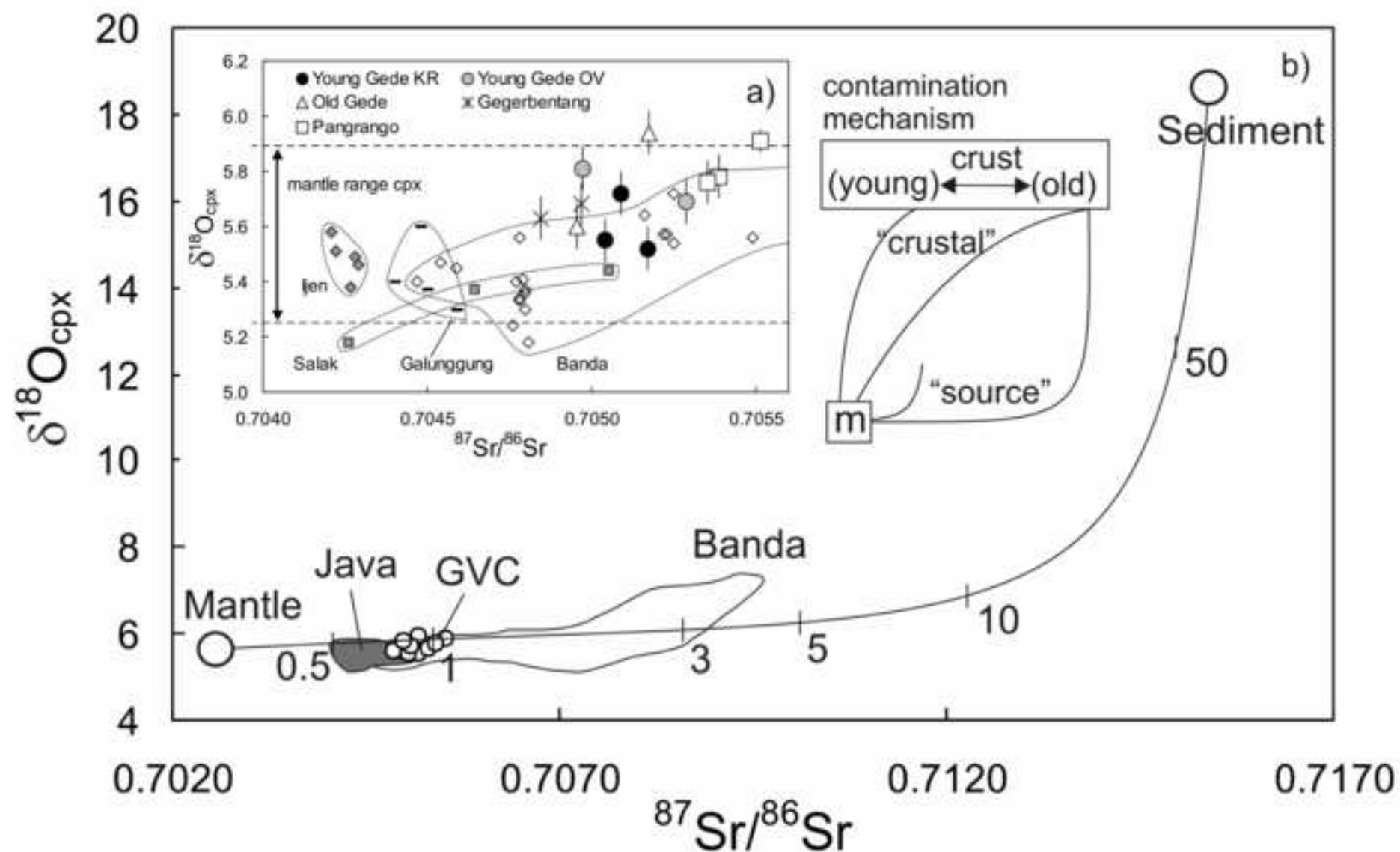


Fig_11
[Click here to download line figure: Fig_11.xls](#)

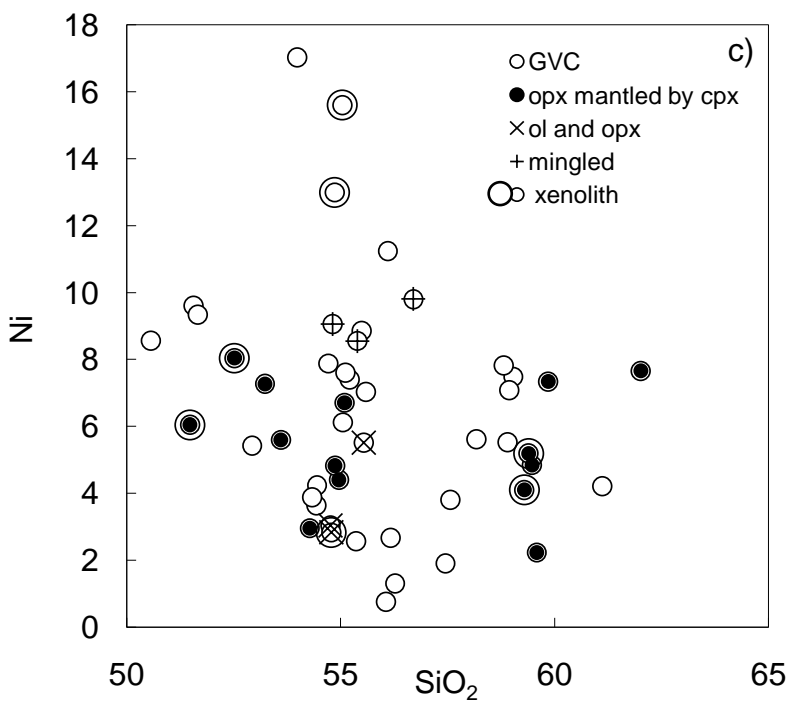
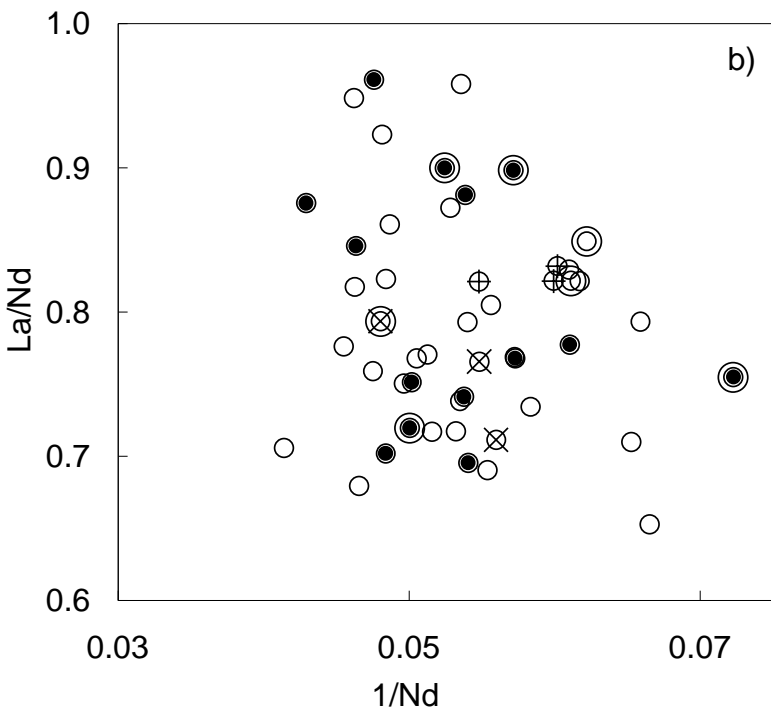
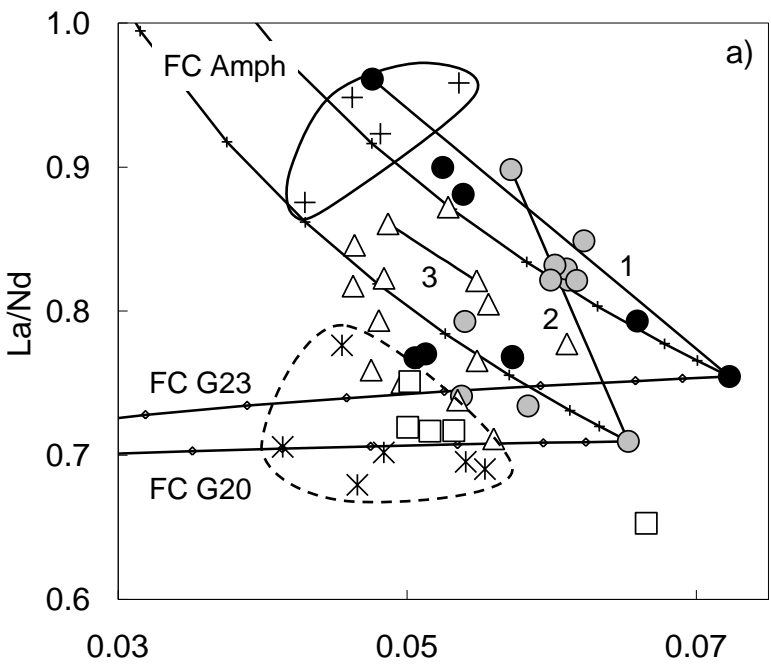


Table 1. Estimated average temperatures and pressures for GVC magma using the two-pyroxene approach

Stratigraphic Group	B/BA/A	Sample	Brey and Kohler (1990) T(°C)	Putirka (2008) Eqn 36, T(°C)	Putirka (2008) Eqn 39, P(kbar)	equivalent depth (km)	n _(eqm)	n _(comb)	% in eqm	Mantled
YGKR	BA	G41	955	1008	3.4	13	4	16	25	N
YGKR	BA	G23	-	-	-	-	0	32	0	Y
YGKR	A	G22	891	962	5.5	21	3	20	15	Y
YGKR	A	G40	958	1046	6.1	23	8	24	33	N
YGOV	BA	G44	995	1018	5.0	19	18	42	43	Y
YGOV	BA	G51	-	-	-	-	0	4	0	N
OG	BA	G37A	951	998	4.5	17	1	14	7	N
OG	BA	G48 ^a	969	1005	5.6	21	8	12	67	N
OG	A	G17	937	984	6.5	24	1	12	8	N
Pang	BA	G24	991	1033	4.8	18	10	20	50	Y
Geg	BA	G27	1014	1026	6.0	22	7	12	58	N
OQ	A	G49	-	-	-	-	0	52	0	Y
Average		All	984	1023	5.5	20	60	260	23	

n_(eqm) = number of two-pyroxene combinations in each sample in equilibrium. Test for equilibrium: KD (Fe-Mg) should be 1.09 ± 0.14.

n_(comb) = number of two-pyroxene combinations tried in each sample.

Mantled = observed overgrowths of clinopyroxene on orthopyroxene: Y, yes; N, no.

Equation 39 uses equation 36 for the temperature input. Calculated pressure for pyroxenes +/- 2.8 kbar (Putirka, 2008).

^a other petrographic disequilibrium texture observed: coexistence of olivine and opx.

B, basalt; BA, basaltic andesite; A, andesite.

The conversion of pressures to depths is obtained by solving (iteratively) the coupled system:

$$\rho(z) = \rho_0 - \rho_0 \alpha (T - T_0) + \rho_0 \beta (P - P_0)$$

$$P(z) = g \int_0^z \rho(z) dz$$

where ρ_0 is a reference density at surface conditions (i.e. T_0 , P_0), α the coefficient of thermal expansion [K⁻¹], and β the compressibility [Pa⁻¹]. Integration is performed from surface downwards. Representative values for all parameters are taken from Schön (2004).

Table 2. Major and trace element data of GVC volcanic rocks

Sample	G01A	G01B	G03	G04	G06	G07	G10	G11	G14	G15	G16	G17	G18	G19	G20	G21	G22
SiO ₂	55.04	54.86	55.21	56.10	55.54	56.27	55.11	56.70	59.03	59.58	51.48	61.11	59.39	55.49	53.98	55.05	59.47
Al ₂ O ₃	18.34	18.53	18.41	18.83	20.65	19.43	20.17	18.04	17.49	20.55	19.41	17.72	17.76	20.02	17.05	18.77	17.34
Fe ₂ O ₃	8.35	8.30	8.18	8.10	7.22	7.78	7.66	8.19	6.93	4.71	10.50	6.57	6.96	7.61	10.33	8.22	7.19
MgO	3.98	4.06	3.95	3.63	2.36	2.50	2.86	3.73	2.93	1.24	4.21	2.54	3.03	2.87	5.22	3.61	3.13
CaO	8.78	8.92	8.79	8.10	8.70	7.60	8.23	8.08	7.06	7.13	9.26	6.15	7.27	8.38	7.50	8.72	7.23
Na ₂ O	2.97	2.96	2.99	3.01	3.53	3.91	3.12	2.94	3.11	3.51	2.77	3.34	3.22	3.14	2.61	3.07	3.21
K ₂ O	1.36	1.32	1.37	1.35	1.06	1.45	1.18	1.41	1.67	1.44	1.18	1.53	1.73	1.27	1.29	1.02	1.74
TiO ₂	0.91	0.91	0.90	0.81	0.81	0.83	0.80	0.81	0.70	0.55	1.08	0.62	0.71	0.79	0.94	0.80	0.74
MnO	0.15	0.15	0.15	0.14	0.14	0.16	0.15	0.15	0.14	0.11	0.20	0.14	0.14	0.15	0.19	0.16	0.14
P ₂ O ₅	0.14	0.14	0.14	0.17	0.22	0.24	0.19	0.15	0.14	0.18	0.18	0.17	0.14	0.19	0.16	0.16	0.14
LOI	0.09	0.15	0.16	0.05	-0.07	-0.02	0.80	0.04	0.89	0.95	-0.15	0.32	-0.20	0.18	0.89	0.47	0.00
Total	100.10	100.29	100.24	100.29	100.16	100.16	100.26	100.24	100.08	99.94	100.12	100.21	100.15	100.08	100.16	100.05	100.32
Sc	30	30	31	20	18	18	17	21	17	9	29	13	19	16	27	22	20
Ti	5467	5556	5898	4909	5017	5455	4939	4406	3878	3518	6683	3465	4256	4316	5814	4957	4621
V	238	246	255	167	135	137	132	185	146	61	245	115	158	130	228	201	173
Cr	17.4	18.2	17.4	9.9	4.0	3.2	8.8	14.0	11.4	2.2	6.2	3.7	6.2	14.6	26.5	5.1	8.4
Mn	1185	1185	1046	1154	1154	1162	1216	1224	1115	751	1603	1162	1076	1208	1557	1324	1162
Co	24	25	26	22	17	19	19	23	19	8	29	15	19	18	31	22	19
Ni	15.6	13.0	7.4	11.2	5.5	1.3	7.6	9.8	7.5	2.2	6.1	4.2	5.2	8.9	17.0	6.1	4.9
Cu	12	15	16	54	52	63	48	25	38	11	72	17	21	49	50	21	23
Zn	76	76	70	77	77	85	67	77	71	56	95	68	69	70	88	82	75
Ga	18	19	19	19	20	21	19	18	18	19	21	18	18	19	18	19	18
Rb	49.6	49.0	50.4	53.4	36.0	54.3	46.7	57.0	70.2	54.2	34.1	58.5	62.1	50.7	57.3	37.0	66.2
Sr	323	319	334	331	397	336	357	287	285	407	301	317	302	337	280	362	307
Y	22	22	23	25	24	31	26	25	26	26	32	22	23	25	24	21	24
Zr	108	107	108	122	102	130	128	128	151	149	116	142	117	124	120	100	138
Nb	4.22	4.18	4.20	4.85	4.26	5.37	4.78	4.72	5.39	5.82	5.25	5.90	4.92	4.73	4.47	3.98	5.09
Cs	3.33	3.31	3.24	2.59	1.68	3.89	3.44	3.91	4.77	3.88	2.55	1.99	2.11	2.59	4.19	2.39	4.41
Ba	250	247	249	254	216	267	238	266	320	317	242	315	313	237	229	211	418
La	13.6	13.4	13.6	14.7	12.7	15.1	13.8	15.0	17.7	18.2	14.4	16.5	15.7	12.6	10.9	12.0	16.4
Ce	28.6	28.5	28.7	32.1	27.8	33.0	30.8	32.1	37.4	39.1	31.5	34.5	32.4	28.1	27.2	26.0	34.3
Pr	3.78	3.76	3.78	4.31	3.94	4.55	4.26	4.24	4.89	5.10	4.40	4.49	4.19	3.87	3.39	3.52	4.44
Nd	16.1	16.4	16.4	18.5	17.9	20.2	18.7	18.2	20.5	21.6	20.0	18.9	17.5	17.1	15.3	15.2	18.6
Sm	3.76	3.80	3.79	4.32	4.19	4.78	4.37	4.16	4.60	4.67	4.96	4.08	3.92	4.09	3.82	3.50	4.05
Eu	1.06	1.07	1.07	1.17	1.26	1.38	1.25	1.14	1.17	1.30	1.33	1.15	1.04	1.24	1.13	1.08	1.05
Gd	3.98	4.09	3.99	4.48	4.36	5.06	4.68	4.39	4.69	4.67	5.35	4.03	3.98	4.23	4.07	3.84	4.10
Tb	0.63	0.63	0.63	0.71	0.69	0.82	0.74	0.69	0.73	0.73	0.88	0.62	0.64	0.69	0.68	0.59	0.65
Dy	3.71	3.77	3.74	4.15	4.03	4.91	4.34	4.05	4.30	4.15	5.25	3.67	3.66	4.10	4.05	3.46	3.81
Ho	0.77	0.78	0.77	0.86	0.83	1.03	0.89	0.85	0.89	0.85	1.09	0.75	0.76	0.84	0.84	0.73	0.80
Er	2.07	2.11	2.12	2.30	2.27	2.82	2.45	2.29	2.43	2.34	2.99	2.10	2.09	2.33	2.33	2.01	2.19
Tm	0.32	0.33	0.33	0.36	0.36	0.44	0.38	0.35	0.39	0.37	0.46	0.33	0.32	0.33	0.38	0.31	0.34
Yb	2.02	2.05	2.09	2.27	2.26	2.84	2.44	2.28	2.46	2.40	2.92	2.15	2.07	2.35	2.41	2.01	2.20
Lu	0.33	0.34	0.34	0.37	0.37	0.47	0.41	0.38	0.40	0.40	0.48	0.36	0.34	0.39	0.40	0.33	0.37
Hf	2.90	2.92	2.94	3.29	2.72	3.46	3.43	3.45	4.08	3.91	3.22	3.71	3.21	3.38	3.27	2.66	3.64
Ta	0.35	0.33	0.34	0.38	0.31	0.41	0.35	0.38	0.44	0.43	0.40	0.44	0.40	0.35	0.34	0.30	0.41
Pb (total)	10.5	10.3	10.4	11.4	7.2	13.0	6.6	12.8	14.2	13.6	11.7	11.3	9.5	10.4	7.5	8.8	12.6
Th	5.48	5.47	5.53	5.78	3.73	5.46	5.40	6.21	7.68	6.46	5.50	6.24	6.61	5.30	5.23	4.10	7.15
U	1.22	1.20	1.23	1.33	0.88	1.32	1.22	1.41	1.75	1.46	1.16	1.39	1.50	1.23	1.25	0.92	1.63

Table 2 continued. Major and trace element data of GVC volcanic rocks

Sample	G23	G24	G25	G26	G27	G28	G29	G30	G31	G32	G33	G35	G36A	G36B	G37A	G38	G39
SiO ₂	52.52	54.87	59.29	53.60	52.93	54.43	51.66	51.56	56.06	54.33	53.23	50.56	54.71	54.81	56.17	55.36	62.01
Al ₂ O ₃	19.19	18.61	17.55	18.89	19.65	18.63	19.33	18.56	21.15	19.63	19.35	19.29	18.52	18.63	20.91	18.76	17.46
Fe ₂ O ₃	9.07	9.42	6.94	9.85	9.65	9.55	10.04	10.34	6.65	8.71	9.59	10.56	8.18	8.29	6.51	8.61	6.13
MgO	4.51	3.64	2.97	3.88	3.51	3.49	4.59	4.98	2.03	2.93	3.70	4.89	4.01	4.11	2.03	3.33	2.52
CaO	9.86	8.43	7.16	8.83	8.97	8.69	9.38	9.67	8.79	8.61	8.76	9.78	8.95	8.91	8.53	7.67	6.22
Na ₂ O	2.75	3.07	3.21	3.09	3.07	3.11	2.82	2.70	3.41	3.28	3.05	2.94	2.89	2.93	3.28	3.08	3.37
K ₂ O	0.91	1.05	1.76	0.93	0.89	1.01	0.81	1.19	1.13	1.00	0.87	0.92	1.30	1.32	1.38	1.14	1.84
TiO ₂	0.90	0.87	0.72	0.89	0.95	0.91	0.96	1.06	0.70	0.79	0.92	1.15	0.91	0.90	0.72	0.85	0.64
MnO	0.17	0.19	0.14	0.20	0.19	0.20	0.18	0.18	0.14	0.19	0.19	0.18	0.14	0.15	0.13	0.17	0.13
P ₂ O ₅	0.13	0.23	0.14	0.23	0.28	0.29	0.21	0.18	0.20	0.29	0.26	0.15	0.13	0.14	0.18	0.19	0.15
LOI	0.07	-0.17	-0.08	-0.23	-0.05	-0.21	-0.13	-0.40	-0.11	0.02	0.20	-0.43	0.22	0.05	0.51	0.97	-0.19
Total	100.08	100.21	99.79	100.16	100.04	100.10	99.86	100.02	100.16	99.78	100.12	100.00	99.96	100.23	100.35	100.12	100.27
Sc	30	21	19	20	19	19	26	32	13	13	19	36	30	30	14	20	13
Ti	5712	5496	4567	5898	6132	5682	6156	6713	4633	4501	5706	7636	5688	5113	4160	5556	3554
V	257	192	167	192	166	152	221	259	108	151	184	316	252	262	128	193	119
Cr	8.3	2.6	6.6	5.6	10.2	4.6	12.6	10.9	1.5	2.6	10.4	15.6	17.3	17.9	1.2	4.6	10.9
Mn	1371	1557	1146	1820	1781	1619	1541	1518	1022	1549	1541	1688	1200	1200	1092	1200	1053
Co	29	24	19	25	22	21	28	32	15	20	24	33	26	26	16	22	15
Ni	8.0	4.8	4.1	5.6	5.4	3.6	9.3	9.6	0.8	3.9	7.3	8.6	7.9	9.1	2.7	2.6	7.7
Cu	48	42	25	39	24	80	36	104	35	41	42	73	14	15	40	36	41
Zn	81	89	74	79	79	88	87	96	77	89	88	84	77	77	71	79	60
Ga	19	20	19	20	20	20	20	20	21	21	20	21	19	19	21	20	17
Rb	32.4	38.7	68.8	31.9	34.0	39.1	30.9	45.8	45.0	35.1	30.4	30.0	48.8	49.8	55.0	43.4	77.0
Sr	354	353	316	406	438	422	397	302	367	405	423	326	324	301	342	351	309
Y	21	27	24	26	30	24	30	31	26	24	27	22	23	29	27	23	26
Zr	80	114	143	98	103	125	83	110	138	103	91	82	108	110	138	122	146
Nb	3.46	5.27	5.22	4.45	5.82	6.98	4.53	4.96	5.52	5.49	4.99	3.72	4.15	4.21	5.85	4.91	5.57
Cs	2.28	1.44	4.55	0.91	1.52	1.11	1.78	1.01	2.31	1.61	1.27	0.84	2.27	3.29	4.24	3.26	2.29
Ba	183	233	330	179	177	212	168	212	210	223	188	160	245	250	307	251	333
La	10.4	15.0	17.2	12.6	14.6	17.1	12.5	13.5	13.9	17.1	14.5	9.8	13.3	13.7	17.7	15.2	21.0
Ce	22.6	32.8	35.9	28.8	32.0	38.6	27.7	29.9	30.5	36.3	31.7	22.2	28.2	29.1	36.9	32.1	44.0
Pr	3.07	4.51	4.61	4.09	4.74	5.38	3.98	4.17	4.31	5.05	4.59	3.22	3.76	3.86	5.04	4.52	5.55
Nd	13.8	19.9	19.1	18.5	21.5	24.1	18.1	18.8	19.4	22.0	20.7	15.0	16.2	16.7	21.6	19.8	22.9
Sm	3.34	4.53	4.22	4.30	5.04	5.47	4.21	4.72	4.70	4.80	4.07	3.89	3.80	3.86	4.84	4.47	4.47
Eu	1.04	1.32	1.08	1.34	1.51	1.54	1.30	1.25	1.36	1.47	1.21	1.08	1.09	1.08	1.35	1.26	1.11
Gd	3.60	4.60	4.28	4.46	5.11	5.44	4.37	5.16	5.02	4.69	4.76	4.35	4.00	4.08	5.06	4.75	4.75
Tb	0.58	0.75	0.68	0.68	0.81	0.84	0.68	0.83	0.82	0.72	0.73	0.73	0.64	0.65	0.78	0.75	0.69
Dy	3.44	4.38	3.93	4.17	4.73	4.87	3.96	4.93	4.91	4.06	4.10	4.42	3.75	3.78	4.54	4.40	3.30
Ho	0.72	0.91	0.81	0.86	1.00	1.00	0.82	1.02	1.03	0.83	0.85	0.93	0.77	0.79	0.96	0.93	0.69
Er	1.96	2.50	2.24	2.39	2.71	2.76	2.24	2.78	2.85	2.24	2.25	2.56	2.09	2.12	2.63	2.55	2.20
Tm	0.30	0.40	0.35	0.38	0.42	0.43	0.34	0.43	0.45	0.35	0.34	0.39	0.32	0.33	0.40	0.39	0.30
Yb	1.92	2.55	2.25	2.39	2.72	2.77	2.15	2.66	2.87	2.23	2.15	2.49	2.05	2.09	2.57	2.55	2.22
Lu	0.31	0.42	0.36	0.40	0.47	0.46	0.36	0.43	0.47	0.37	0.35	0.41	0.33	0.34	0.43	0.43	0.30
Hf	2.20	3.04	3.77	2.65	2.79	3.28	2.27	3.04	3.68	2.76	2.49	2.33	2.91	2.96	3.62	3.25	3.34
Ta	0.26	0.37	0.43	0.29	0.35	0.43	0.30	0.37	0.40	0.35	0.31	0.26	0.33	0.33	0.43	0.36	0.30
Pb (total)	8.3	18.1	12.9	5.1	6.7	12.2	8.2	14.4	9.7	7.7	8.9	5.1	10.4	10.7	13.9	9.9	11.0
Th	3.45	4.50	7.43	3.73	3.32	4.14	3.14	5.16	4.64	4.32	3.41	3.21	5.34	5.51	6.06	4.82	8.08
U	0.78	1.06	1.70	0.86	0.80	1.01	0.74	1.17	1.09	1.00	0.82	0.73	1.18	1.24	1.44	1.12	1.44

Table 3. Whole-rock Sr isotope data of GVC volcanic rocks

Sample	⁸⁷ Sr/ ⁸⁶ Sr _m	2SE
G01A	0.705325	0.000009
G01B	0.705288	0.000009
G10	0.705004	0.000010
G16	0.705540	0.000012
G17	0.704990	0.000009
G18	0.705143	0.000009
G19	0.704980	0.000013
G20	0.705088	0.000011
G21	0.705118	0.000008
G22	0.705140	0.000011
G23	0.705268	0.000011
G25	0.705117	0.000010
G26	0.704882	0.000011
G28	0.705056	0.000011
G30	0.705393	0.000013
G33	0.704997	0.000008
G35	0.705358	0.000009
G36A	0.705318	0.000012
G40	0.705070	0.000010
G42	0.705207	0.000009
G44	0.705001	0.000009
G46	0.705201	0.000012
G49	0.704735	0.000008
G51	0.705294	0.000012
G52	0.704508	0.000009
G55	0.705057	0.000009

_m = measured
2SE: 2*standard internal error

Table 4. Oxygen isotope data
($\delta^{18}\text{O}$) of GVC mineral separates

	CPX	OL	PLAG
G01A	5.69	5.39	
G16	5.91		
G17	5.60		
G25	5.72		
G26	5.63		6.07
G30	5.78	5.42	
G35	5.76	5.32	
G33	5.68		
G40	5.55		
G42	5.52		
G44	5.81		
G46	5.94		

CPX, clinopyroxene; OL, olivine;
PLAG, plagioclase.

Table 5. Results of least squares major element modelling

Model	Parent		Daughter		SiO ₂ range	Σr^2	Plag	Cpx	Ol	Opx	Ox	%C
1	G29	GEG	G28	GEG	52-54	0.07	26.1	1.51		9	2.23	39
2	G29	GEG	G32	GEG	52-54	0.09	23.8	3.46		9.2	2.45	39
3	G35	PAN	G31	PAN	51-56	0.07	26	7.79	8.05		3.61	45
4	G35	PAN	G24	PAN	51-55	0.10	31.7	5.42	6.47		2.95	47
5	G48	OG	G17	OG	55-61	0.09	25.9	0.57		8.34	3.34	38
6	G48	OG	G15	OG	55-60	0.05	14.9	2.96		9.89	3.54	31
7	G20	YGOV	G18	YGOV	54-59	0.03	8.79	1.27		6.74	3.01	20
8	G36A	YGOV	G18	YGOV	55-59	0.06	15.7	4.2		2.83	1.94	25
9	G20	YGOV	G19	YGOV	54-55	0.10	8.56	3.37		5.17	1.15	1
10	G23	YGKR	G39	YGKR	53-62	0.08	33.3	8.1	5.16		3.89	50
11	G23	YGKR	G22	YGKR	53-60	0.06	29.7	5.8	4.75		3.12	43
12	G48	OG	G39	YGKR	55-62	0.03	27.6	0.47		9.15	3.66	40
13	G48	OG	G18	YGOV	55-59	0.03	20.3	2.63		7.73	2.89	28
14	G23	YGKR	G15	OG	53-60	0.06	22.6	11.1	5.4		3.95	43

SiO₂ range in wt %

C% = degree of crystallisation

Plag, plagioclase; Cpx, clinopyroxene; Ol, olivine; Opx, orthopyroxene; Ox, Fe-Ti oxide.

GEG, Gegerbentang; PAN, Pangrango; OG, Old Gede; YGO, Young Gede Other Vents; YGKR, Young Gede Kawah Ratu

Bold font indicates the addition rather than removal of a particular phase.

The mineral phases considered in modelling are limited to those observed as phenocrysts in either the parent or daughter rocks.

Analytical techniques

Mineral analyses were performed on carbon-coated polished thin sections of selected GVC volcanic rocks using a Cameca SX 100 electron microprobe at the University of Manchester NERC facility. The accelerating voltage was 15kV and beam current was 2nA. Detection limits based on counting statistics (wt%) for Al, Mg, K, Ca, Ti are 0.01 or lower, Na, Si, Cr, Ni are around 0.03, while Fe is slightly higher around 0.08. Element precision is dependant on the mineral being analysed but was typically better than 1% for Ca, Ti, Si, Al and Mg, between 1-2% for Fe, 2.7% for Ni and around 4% for Na, K, Mn and Cr.

Major element contents of GVC whole-rock samples were determined on fused glass discs produced by the Fusion method (spectroflux 105) using the Automated Philips PW2404 X-ray fluorescence spectrometer at the University of Edinburgh. In-house rock standards were used to calibrate the machine and monitor accuracy and precision during analysis.

Trace element concentrations of GVC rock powders were determined on the PerkinElmer ELAN 6000 quadrupole ICP-MS at Durham University following the analytical procedure and instrument operating conditions described by Ottley et al. (2003). Multiple analyses of procedural blanks (3 per batch), in-house standards and international reference materials (W2, BHVO-1, AGV1, BE-N and BIR1) during each session e.g. at the start, mid-way and at the end of a run, allowed any drift in the instrument calibration to be detected. Reproducibility (internal and external) of standard values on the ELAN were better than 5% relative standard deviation.

Preparation of whole rock powders for Sr isotope analysis was undertaken in the Arthur Holmes Isotope Geology Laboratory (AHIGL) at Durham University. The separation procedure for Sr follows that detailed by Handley et al. (2008a). Sr isotope ratios were determined on the AHIGL ThermoElectron Neptune Multi-collector Plasma Mass Spectrometer (MC-ICP-MS). Details of instrument operating conditions are presented in Nowell et al. (2003) and Dowall et al. (2003). Instrumental mass bias was corrected for using a $^{88}\text{Sr}/^{86}\text{Sr}$ ratio of 8.375209 (the reciprocal of the $^{86}\text{Sr}/^{88}\text{Sr}$ ratio of 0.1194). Data quality was monitored over several analytical sessions by regular analysis of standard reference materials during each run. The reproducibility of the $^{87}\text{Sr}/^{86}\text{Sr}$ ratios for NBS 987 standard solutions in each of the individual analytical sessions is better than 21 ppm in all cases. Blank samples processed (at

least 2 per sample batch) were analysed by ICP-MS on the PerkinElmer ELAN 6000 quadrupole at Durham University. Total analytical blanks for Sr were below 1.2 ng (typically <300 pg). These values are insignificant considering the quantity of Sr processed from the volcanic rocks (30-66 µg).

Oxygen isotope analyses of mineral separates (~10mg per sample) were determined by laser-fluorination at Royal Holloway, University of London using an analytical procedure following that of Macpherson et al. (2000). In-house standard values of SC olivine 2 and GMG II during the period of study were within 0.01‰ of accepted values: +5.24‰ ± 0.04 (1σ, n = 6) and +5.69‰ ± 0.08 (1σ, n = 15), respectively. Oxygen yields were slightly low, but consistent over the individual sessions: 93% for plagioclase (n = 1), between 92-94% (n = 12) for clinopyroxene and between 98-100% for olivine (n = 3). Replicate analyses of plagioclase and clinopyroxene throughout the study were within 0.09‰ and 0.04‰ respectively. Oxygen results are reported as per mil deviations relative to the standard mean ocean water (V-SMOW) standard.

References

- Handley HK, Davidson JP, Macpherson CG (2008a) Untangling differentiation in arc lavas: constraints from unusual minor and trace element variations at Salak Volcano, Indonesia. *Chem Geol* 255:360-376
- Macpherson CG, Hilton DR, Matthey DP, Sinton JM (2000). Evidence for an ¹⁸O-depleted mantle plume from contrasting ¹⁸O/¹⁶O ratios of back-arc lavas from the Manus Basin and Mariana Trough. *Earth Planet Sci Lett* 176:171-183.
- Nowell GM, Pearson DG, Ottley CJ, Schweiters J (2003) Long-term performance characteristics of a plasma ionisation multi-collector mass spectrometer (PIMMS): the ThermoFinnigan Neptune. *Plasma Source Mass Spectrometry. Spec Pub Royal Soc Chem* 307-320.
- Ottley CJ, Pearson DG, Irvine GJ (2003) A routine method for the dissolution of geological samples for the analysis of REE and trace elements via ICP-MS. *Plasma Source Mass Spectrometry. Spec Pub Royal Soc Chem* 221-230.

Supplementary Table 1. Modal proportions of mineral phases in GVC volcanic rocks

	G01A	G01B	G04	G06	G07	G08	G09	G10
OI	3.2	4.1	-	1.2	8.5	11.8	11.1	-
Opx	-	-	5.2	3.1	-	-	-	1.1
Cpx	8.3	9.8	10.7	6.9	3.2	3.1	7.3	4.9
Plag	26.5	31.2	44.3	57.3	64.8	31.7	57.7	31.3
Ox	1.5	-	0.8	3.1	1.2	1.5	1.9	0.8
Hbl	-	-	-	-	-	-	-	-
Bio	-	-	-	-	-	-	-	-
GM	60.5	54.9	39.0	28.4	22.3	51.9	22.0	61.9
	G13(light)	G13(dark)	G15	G16	G17	G18	G19	G20
OI	-	3.9	-	8.8	-	-	-	-
Opx	3.8	3.2	4.3	1.1	12.1	8.2	4.5	3.2
Cpx	10.8	8.7	2.8	13.3	6.3	10.6	7.2	16.2
Plag	38.4	41.3	53.9	53.8	39.5	42.3	30.4	27.6
Ox	2.4	1.8	1.8	2.2	2.8	2.8	1.1	2.7
Hbl	-	-	-	-	-	-	-	-
Bio	-	-	-	-	-	-	-	-
GM	44.6	41.1	37.2	20.8	39.3	36.1	56.8	50.3
	G21	G22	G24	G25	G26	G27	G28	G29
OI	-	-	-	-	3.7	-	-	10.9
Opx	3.4	5.3	7.2	9.2	2.1	6.2	5.3	-
Cpx	13.6	11.0	19.5	11.2	19.7	8.5	15.6	14.1
Plag	52.8	48.4	37.1	41.5	31.7	41.4	29.7	50.4
Ox	1.5	3.2	4.0	2.2	3.8	3.7	2.1	1.3
Hbl	-	-	-	-	-	-	-	-
Bio	-	-	-	-	-	-	-	-
GM	28.7	32.1	32.2	35.9	39.0	40.2	47.3	23.3
	G30	G31	G32	G33	G35	G36A	G36B	G37A
OI	8.3	-	-	-	12.2	10.4	7.6	-
Opx	-	3.2	3.1	7.2	-	-	-	3.1
Cpx	22.4	14.3	14.8	10.5	9.1	19.2	17.1	5.4
Plag	34.9	35.3	35.3	41.3	34.4	27.7	21.7	31.3
Ox	2.1	3.1	2.8	2.4	1.3	1.4	1.3	1.9
Hbl	-	-	-	-	-	-	-	-
Bio	-	-	-	-	-	-	-	-
GM	32.3	44.1	44.0	38.6	43.0	41.3	52.3	58.3
	G37B	G38	G39	G40	G41	G42	G43	G44
OI	-	-	-	-	-	-	-	-
Opx	3.2	6.3	12.4	18.2	10.4	20.2	4.9	10.0
Cpx	7.3	11.0	9.0	10.2	7.3	5.7	17.0	6.1
Plag	39.5	32.3	45.2	34.1	46.3	39.5	37.3	25.7
Ox	0.9	1.2	2.7	2.7	0.5	1.3	1.2	1.1
Hbl	-	-	-	-	-	-	-	-
Bio	-	-	-	-	-	-	-	-
GM	49.1	49.2	30.7	34.8	35.5	33.3	39.6	57.1
	G45	G46	G47	G48	G49	G50A	G51(dark)	G51(light)
OI	-	-	-	3.2	-	-	3.2	-
Opx	0.8	0.5	3.1	2.1	4.2	4.9	-	0.5
Cpx	4.2	5.3	3.5	4.8	6.2	2.3	17.1	1.1
Plag	44.6	38.5	44.2	34.7	42.7	37.4	30.6	11.8
Ox	2.3	3.2	1.6	1.1	3.2	1.2	3.0	0.5
Hbl	-	-	-	-	-	-	-	-
Bio	-	-	-	-	-	-	-	-
GM	48.1	52.5	47.6	54.1	43.7	54.2	46.1	86.1
	G52	G53	G54	G55	G56	G57	G58	
OI	-	-	-	0.5	0.5	-	-	
Opx	2.1	3.2	2.1	0.9	6.1	12.1	7.2	
Cpx	8.7	6.9	13.4	2.1	3.2	4.0	16.8	
Plag	63	42.6	48.2	17.5	51.7	59.6	45.7	
Ox	2	3.1	4.3	2.3	4.1	1.1	1.0	
Hbl	0.5	-	-	-	-	-	-	
Bio	-	-	-	0.4	-	-	-	
GM	23.7	44.2	32.0	76.3	34.4	23.2	29.3	

Modal phase volume (%) established from point-counting between 200 and 300 points per sample for microphenocrysts (100-300mm) and phenocrysts (>300mm).
OI, olivine; Opx, orthopyroxene; Cpx, clinopyroxene; Plag, plagioclase; Ox, Fe-Ti oxide; Hbl, hornblende; Bio, biotite; GM, groundmass.

Supplementary Table 2. Representative plagioclase mineral data

Sample	G01B	G01B	G01B	G01B	G11	G11	G11	G11	G11	G22	G22	G22	G23
Grain	P1	P1	P1	GM	P2	P2	P4	P4	P4	P2	P2	P2	P1
Position	C	M	R		C	R	C	M	R	C	M	R	
SiO ₂	43.43	44.08	44.84	47.03	48.25	47.47	53.68	53.04	54.80	47.25	46.67	48.93	48.31
TiO ₂	0.02	0.01	0.02	0.03	0.02	0.02	0.03	0.05	0.03	0.03	0.03	0.03	0.03
Al ₂ O ₃	34.45	33.91	33.44	32.29	31.61	31.73	28.40	28.44	27.31	32.13	32.70	31.03	31.77
Cr ₂ O ₃	0.02	0.01	0.01	0.01	0.00	0.00	0.00	0.00	0.01	0.00	0.01	0.01	0.00
MgO	0.04	0.04	0.06	0.08	0.10	0.06	0.05	0.06	0.07	0.03	0.04	0.06	0.08
CaO	19.48	19.36	18.51	17.03	16.74	16.65	12.51	12.74	11.43	16.74	17.29	15.74	16.41
MnO	0.00	0.00	0.00	0.00	0.00	0.00	0.02	0.00	0.00	0.02	0.00	0.00	0.00
FeO	0.48	0.42	0.57	0.80	0.73	0.65	0.60	0.59	0.62	0.53	0.47	0.65	0.65
NiO	0.00	0.02	0.00	0.00	0.00	0.01	0.01	0.00	0.01	0.01	0.00	0.01	0.00
Na ₂ O	0.73	0.87	1.36	2.12	2.06	2.33	4.44	4.30	4.97	2.30	1.94	2.87	2.56
K ₂ O	0.01	0.01	0.03	0.06	0.17	0.06	0.27	0.27	0.30	0.08	0.05	0.09	0.05
Total	98.65	98.72	98.83	99.44	99.67	98.97	100.01	99.50	99.55	99.12	99.21	99.42	99.87
Si	8.18	8.29	8.41	8.74	8.92	8.84	9.76	9.70	9.98	8.79	8.68	9.05	8.91
Al	7.65	7.52	7.40	7.07	6.88	6.96	6.08	6.13	5.86	7.04	7.17	6.76	6.90
Fe(ii)	0.08	0.07	0.09	0.12	0.11	0.10	0.09	0.09	0.08	0.08	0.07	0.10	0.10
Ca	3.93	3.90	3.72	3.39	3.31	3.32	2.44	2.50	2.23	3.34	3.45	3.12	3.24
Na	0.27	0.32	0.49	0.76	0.74	0.84	1.57	1.52	1.76	0.83	0.70	1.03	0.92
K	0.00	0.00	0.01	0.01	0.04	0.01	0.06	0.06	0.07	0.02	0.01	0.02	0.01
Mg	0.01	0.01	0.02	0.02	0.03	0.02	0.01	0.02	0.02	0.01	0.01	0.02	0.02
Total	20.12	20.11	20.13	20.11	20.03	20.10	20.01	20.02	20.00	20.11	20.09	20.09	20.10
An	93.57	92.44	88.17	81.35	80.94	79.51	59.92	61.16	54.99	79.68	82.89	74.80	77.74
Ab	6.37	7.51	11.68	18.33	18.06	20.17	38.52	37.31	43.30	19.85	16.84	24.68	21.95
Or	0.06	0.05	0.15	0.32	1.00	0.32	1.56	1.53	1.71	0.46	0.27	0.52	0.30

Sample	G23	G23	G23	G24	G24	G26	G26	G26	G30	G30	G30	G30	G30
Grain	P3	P4	P4	P1	P1	P1	P1	GM	P1	P1	P1	P2	P2
Position	R	C-M	R	C	M	C	R		C	M	R	C	R
SiO ₂	48.13	47.63	48.86	51.40	50.48	48.73	50.93	52.52	48.48	46.27	49.11	48.38	50.36
TiO ₂	0.05	0.03	0.06	0.00	0.04	0.03	0.05	0.05	0.04	0.04	0.04	0.04	0.06
Al ₂ O ₃	30.95	31.52	30.80	28.84	28.93	30.76	29.27	28.77	31.45	32.31	30.21	31.15	28.98
Cr ₂ O ₃	0.01	0.00	0.00	0.00	0.01	0.00	0.01	0.00	0.01	0.00	0.01	0.00	0.02
MgO	0.10	0.07	0.25	0.08	0.08	0.06	0.05	0.06	0.07	0.07	0.10	0.08	0.08
CaO	16.00	16.49	15.60	13.08	13.49	15.20	13.77	12.82	16.00	16.53	14.83	15.88	13.71
MnO	0.00	0.00	0.02	0.00	0.01	0.00	0.01	0.00	0.03	0.02	0.00	0.02	0.00
FeO	0.73	0.58	0.82	0.59	0.60	0.72	0.95	0.86	0.56	0.52	0.74	0.67	0.90
NiO	0.00	0.00	0.00	0.00	0.00	0.01	0.00	0.00	0.00	0.01	0.00	0.00	0.02
Na ₂ O	2.78	2.47	2.81	4.22	3.94	3.18	3.87	4.54	2.77	2.35	3.24	2.64	3.83
K ₂ O	0.07	0.06	0.17	0.18	0.16	0.10	0.16	0.22	0.12	0.09	0.17	0.12	0.25
Total	98.81	98.85	99.38	98.38	97.74	98.77	99.07	99.85	99.50	98.21	98.45	98.98	98.19
Si	8.97	8.88	9.05	9.53	9.44	9.07	9.41	9.60	8.97	8.70	9.16	8.99	9.40
Al	6.80	6.92	6.72	6.30	6.38	6.75	6.38	6.20	6.85	7.16	6.64	6.82	6.38
Fe(ii)	0.11	0.09	0.13	0.09	0.09	0.11	0.15	0.13	0.09	0.08	0.12	0.10	0.14
Ca	3.20	3.29	3.10	2.60	2.70	3.03	2.73	2.51	3.17	3.33	2.96	3.16	2.74
Na	1.01	0.89	1.01	1.52	1.43	1.15	1.39	1.61	0.99	0.86	1.17	0.95	1.38
K	0.02	0.01	0.04	0.04	0.04	0.02	0.04	0.05	0.03	0.02	0.04	0.03	0.06
Mg	0.03	0.02	0.07	0.02	0.02	0.02	0.01	0.02	0.02	0.02	0.03	0.02	0.02
Total	20.13	20.11	20.11	20.10	20.10	#REF!	20.13	#REF!	20.11	20.16	20.12	20.08	20.13
An	75.78	78.42	74.66	62.51	64.82	72.14	65.66	60.22	75.64	79.10	70.98	76.35	65.51
Ab	23.85	21.27	24.36	36.46	34.28	27.31	33.42	38.55	23.69	20.39	28.04	22.96	33.08
Or	0.37	0.31	0.98	1.03	0.90	0.54	0.91	1.23	0.67	0.51	0.98	0.68	1.42

Sample	G48	G48	G48	G51 L	G51 L	G51 L	G51 L	G51 L	G51 L	G51 D	G51 D	G51 D	G51 D
Grain	P4	P4	P5	P2	P2	P2	P3	P3	P3	P4	P4	P5	GM
Position	C	R	R	C	M	R	C	M	R	C	R	R	R
SiO ₂	54.41	53.07	51.48	46.37	46.96	51.85	44.98	52.66	56.15	45.11	45.15	44.92	45.31
TiO ₂	0.06	0.02	0.00	0.02	0.02	0.03	0.03	0.04	0.04	0.04	0.03	0.03	0.04
Al ₂ O ₃	28.24	28.89	30.44	32.13	31.97	29.41	33.52	27.37	26.34	33.66	32.59	33.45	33.61
Cr ₂ O ₃	0.00	0.00	0.01	0.00	0.00	0.00	0.00	0.00	0.00	0.00	0.00	0.01	0.00
MgO	0.06	0.08	0.08	0.04	0.03	0.04	0.03	0.05	0.05	0.06	0.06	0.05	0.05
CaO	11.94	12.54	14.26	17.19	16.75	13.50	18.69	11.46	10.00	18.61	17.83	18.43	18.55
MnO	0.00	0.00	0.02	0.00	0.00	0.00	0.00	0.00	0.00	0.01	0.00	0.00	0.02
FeO	0.76	0.73	0.72	0.42	0.55	0.51	0.63	0.57	0.52	0.54	0.85	0.56	0.66
NiO	0.00	0.02	0.01	0.00	0.00	0.01	0.00	0.01	0.00	0.01	0.00	0.00	0.00
Na ₂ O	4.85	4.42	3.65	2.06	2.32	3.99	1.28	4.83	5.78	1.26	1.54	1.31	1.23
K ₂ O	0.30	0.21	0.12	0.08	0.08	0.20	0.03	0.28	0.43	0.02	0.02	0.02	0.03
Total	100.63	99.98	100.79	98.31	98.68	99.54	99.18	97.25	99.32	99.31	98.08	98.78	99.50
Si	9.83	9.66	9.34	8.71	8.78	9.50	8.41	9.83	10.21	8.42	8.53	8.43	8.44
Al	6.01	6.20	6.51	7.11	7.04	6.35	7.39	6.02	5.64	7.40	7.26	7.40	7.38
Fe(ii)	0.12	0.11	0.11	0.07	0.09	0.08	0.10	0.09	0.08	0.08	0.13	0.09	0.10
Ca	2.31	2.44	2.77	3.46	3.35	2.65	3.75	2.29	1.95	3.72	3.61	3.70	3.70
Na	1.70	1.56	1.28	0.75	0.84	1.42	0.46	1.75	2.04	0.46	0.56	0.48	0.44
K	0.07	0.05	0.03	0.02	0.02	0.05	0.01	0.07	0.10	0.00	0.01	0.00	0.01
Mg	0.02	0.02	0.02	0.01	0.01	0.01	0.01	0.01	0.01	0.02	0.02	0.01	0.01
Total	20.04	20.04	20.06	20.12	20.13	20.05	20.12	20.06	20.03	20.10	20.12	20.11	20.09
An	56.67	60.34	67.89	81.83	79.60	64.41	88.85	55.83	47.66	89.00	86.42	88.50	89.13
Ab	41.64	38.48	31.41	17.74	19.93	34.45	10.98	42.53	49.88	10.89	13.46	11.38	10.71
Or	1.68	1.19	0.70	0.43	0.46	1.14	0.18	1.64	2.46	0.10	0.12	0.11	0.16

Grain: P, phenocryst; GM, groundmass.
Spot: C, core; M, mid point; R, rim.
An, anorthite; Ab, albite; Or, orthoclase.
Structural formula based on 32 oxygens.

Supplementary Table 3. Representative clinopyroxene mineral data

Sample	G01B	G01B	G01B	G01B	G01B	G11	G11	G11	G17	G17	G17	G22	G22
Grain	P2	P2	P3	P3	GM	P1	P2	INC (Plag P3)	P1	P1	P1	P1	P1
Position	C	R	C	R					C	M	R	C	R
SiO ₂	50.99	49.97	51.30	50.93	48.84	50.48	50.95	50.78	50.95	50.11	49.59	51.58	50.59
TiO ₂	0.51	0.73	0.61	0.67	0.80	0.63	0.58	0.53	0.44	0.64	0.61	0.27	0.55
Al ₂ O ₃	2.01	3.04	2.46	2.77	4.03	2.22	2.19	2.43	1.94	2.53	2.83	1.17	2.31
Cr ₂ O ₃	0.00	0.02	0.00	0.00	0.05	0.00	0.00	0.00	0.00	0.01	0.00	0.00	0.00
Fe ₂ O ₃	4.56	4.66	3.33	3.72	5.37	3.25	2.51	2.43	3.70	3.78	4.41	3.13	3.71
FeO	4.38	3.79	5.44	4.82	3.57	10.55	10.60	10.60	7.69	8.35	8.03	7.92	6.52
MnO	0.26	0.20	0.26	0.24	0.21	0.46	0.45	0.44	0.49	0.42	0.44	0.47	0.35
MgO	15.84	15.10	15.34	15.23	14.82	13.61	13.50	13.12	13.92	13.97	13.56	14.15	14.44
CaO	21.39	22.00	21.61	21.88	21.61	18.71	19.23	19.63	20.80	19.48	19.83	21.09	20.89
Na ₂ O	0.25	0.28	0.25	0.27	0.27	0.36	0.36	0.35	0.36	0.40	0.39	0.28	0.35
K ₂ O	0.00	0.00	0.00	0.00	0.00	0.00	0.00	0.00	0.00	0.00	0.00	0.00	0.00
NiO	0.02	0.03	0.01	0.00	0.00	0.01	0.00	0.00	0.01	0.02	0.00	0.01	0.00
Total	100.20	99.81	100.61	100.54	99.56	100.29	100.37	100.30	100.30	99.70	99.68	100.05	99.71
Si	1.91	1.88	1.91	1.90	1.85	1.91	1.92	1.92	1.92	1.90	1.89	1.95	1.91
Al	0.09	0.13	0.11	0.12	0.18	0.10	0.10	0.11	0.09	0.11	0.13	0.05	0.10
Fe(ii)	0.14	0.12	0.17	0.15	0.11	0.33	0.33	0.33	0.24	0.26	0.25	0.25	0.20
Fe(iii)	0.13	0.13	0.09	0.10	0.15	0.09	0.07	0.07	0.10	0.11	0.13	0.09	0.10
Cr	0.00	0.00	0.00	0.00	0.00	0.00	0.00	0.00	0.00	0.00	0.00	0.00	0.00
Ti	0.01	0.02	0.02	0.02	0.02	0.02	0.02	0.02	0.01	0.02	0.02	0.01	0.02
Mn	0.01	0.01	0.01	0.01	0.01	0.01	0.01	0.01	0.02	0.01	0.01	0.01	0.01
Mg	0.88	0.85	0.85	0.84	0.83	0.77	0.76	0.74	0.78	0.79	0.77	0.80	0.81
Ca	0.86	0.89	0.86	0.87	0.88	0.76	0.78	0.80	0.84	0.79	0.81	0.85	0.85
Na	0.02	0.02	0.02	0.02	0.02	0.03	0.03	0.03	0.03	0.03	0.03	0.02	0.03
Total	4.04	4.04	4.03	4.03	4.05	4.03	4.02	4.02	4.03	4.03	4.04	4.03	4.03
Wo	42.61	44.59	43.48	44.13	44.23	38.61	39.78	40.76	42.38	40.30	41.04	42.64	42.73
En	43.93	42.59	42.96	42.73	42.19	39.10	38.85	37.91	39.46	40.21	39.06	39.80	41.11
Fs	13.46	12.82	13.56	13.14	13.58	22.29	21.37	21.33	18.16	19.49	19.90	17.56	16.16

Sample	G17	G17	G17	G23	G23	G23	G23	G23	G23	G26	G26	G26	G30
Grain	P1	P1	P1	P1	P1	P2	P2	P4*	P4*	P1	P2	P2	P1
Position	C	M	R	C	R	C	R		R		C	R	C
SiO ₂	50.95	50.11	49.59	49.88	50.43	50.18	50.25	49.77	49.84	49.31	49.14	49.26	49.52
TiO ₂	0.44	0.64	0.61	0.75	0.60	0.67	0.78	0.57	0.73	0.75	0.88	0.65	0.84
Al ₂ O ₃	1.94	2.53	2.83	3.53	3.10	2.80	2.71	2.85	3.29	3.33	4.06	3.19	3.42
Cr ₂ O ₃	0.00	0.01	0.00	0.00	0.00	0.00	0.00	0.01	0.01	0.00	0.00	0.01	0.01
Fe ₂ O ₃	3.70	3.78	4.41	4.31	4.37	4.26	3.67	2.69	4.92	5.17	4.71	5.19	4.35
FeO	7.69	8.35	8.03	4.37	4.74	5.81	6.80	7.19	4.70	5.12	5.55	5.76	5.89
MnO	0.49	0.42	0.44	0.26	0.18	0.34	0.34	0.31	0.29	0.35	0.35	0.39	0.32
MgO	13.92	13.97	13.56	14.69	15.62	15.30	14.90	14.07	15.03	14.70	14.24	14.96	14.61
CaO	20.80	19.48	19.83	22.06	20.94	20.22	20.19	20.27	21.18	20.71	20.81	19.70	20.58
Na ₂ O	0.36	0.40	0.39	0.27	0.26	0.28	0.26	0.31	0.29	0.31	0.34	0.30	0.29
K ₂ O	0.00	0.00	0.00	0.00	0.00	0.00	0.00	0.00	0.00	0.00	0.00	0.00	0.00
NiO	0.01	0.02	0.00	0.01	0.03	0.00	0.00	0.01	0.00	0.01	0.00	0.02	0.00
Total	100.30	99.70	99.68	100.12	100.20	99.81	100.61	98.05	100.26	99.77	100.08	99.44	99.83
Si	1.92	1.90	1.89	1.87	1.88	1.89	1.89	1.91	1.87	1.87	1.85	1.87	1.87
Al	0.09	0.11	0.13	0.16	0.14	0.12	0.12	0.13	0.15	0.15	0.18	0.14	0.15
Fe(ii)	0.24	0.26	0.25	0.14	0.15	0.18	0.21	0.23	0.15	0.16	0.17	0.18	0.18
Fe(iii)	0.10	0.11	0.13	0.12	0.12	0.12	0.10	0.08	0.14	0.15	0.13	0.15	0.12
Cr	0.00	0.00	0.00	0.00	0.00	0.00	0.00	0.00	0.00	0.00	0.00	0.00	0.00
Ti	0.01	0.02	0.02	0.02	0.02	0.02	0.02	0.02	0.02	0.02	0.02	0.02	0.02
Mn	0.02	0.01	0.01	0.01	0.01	0.01	0.01	0.01	0.01	0.01	0.01	0.01	0.01
Mg	0.78	0.79	0.77	0.82	0.87	0.86	0.84	0.80	0.84	0.83	0.80	0.85	0.82
Ca	0.84	0.79	0.81	0.89	0.84	0.82	0.81	0.83	0.85	0.84	0.84	0.80	0.83
Na	0.03	0.03	0.03	0.02	0.02	0.02	0.02	0.02	0.02	0.02	0.03	0.02	0.02
Total	4.03	4.03	4.04	4.04	4.04	4.04	4.03	4.02	4.04	4.05	4.04	4.05	4.03
Wo	42.38	40.30	41.04	44.94	42.29	41.07	41.19	42.63	42.92	42.29	42.95	40.31	42.22
En	39.46	40.21	39.06	41.65	43.88	43.25	42.31	41.18	42.36	41.75	40.90	42.60	41.72
Fs	18.16	19.49	19.90	13.40	13.82	15.68	16.50	16.18	14.72	15.96	16.15	17.09	16.05

Sample	G30	G35	G35	G35	G35	G40	G40	G40	G48	G48	G48	G51 L	G51 D
Grain	P2	P1	P2	P3	P3	P1	P2	P3	P1	P2	P3	P1	P2
Position	C			C	R		M						
SiO ₂	48.03	49.57	49.65	50.38	50.83	49.32	49.84	48.43	51.18	51.27	51.31	50.73	50.97
TiO ₂	0.99	0.83	0.97	0.70	0.69	0.53	0.55	0.61	0.67	0.54	0.47	0.49	0.45
Al ₂ O ₃	4.99	4.00	3.66	2.80	1.86	2.60	2.38	2.88	2.10	2.73	2.56	1.42	1.92
Cr ₂ O ₃	0.01	0.01	0.01	0.01	0.00	0.00	0.00	0.02	0.02	0.02	0.00	0.00	0.01
Fe ₂ O ₃	5.34	4.58	3.95	3.83	3.37	4.68	3.64	5.23	2.86	2.27	2.39	3.71	3.53
FeO	5.40	4.98	6.30	6.58	6.84	8.29	7.92	8.17	9.74	10.10	10.75	7.82	9.06
MnO	0.21	0.21	0.31	0.30	0.34	0.44	0.38	0.46	0.47	0.43	0.45	0.42	0.40
MgO	13.75	14.64	14.41	15.00	15.25	13.37	14.14	13.28	14.30	13.51	13.37	14.20	13.59
CaO	20.68	21.11	20.41	19.88	20.16	19.66	19.71	19.03	19.30	19.76	19.58	20.45	20.42
Na ₂ O	0.37	0.37	0.39	0.39	0.26	0.37	0.29	0.38	0.30	0.40	0.36	0.29	0.32
K ₂ O	0.00	0.00	0.00	0.00	0.00	0.00	0.00	0.00	0.00	0.00	0.00	0.00	0.00
NiO	0.00	0.00	0.00	0.01	0.01	0.00	0.00	0.02	0.02	0.00	0.01	0.02	0.01
Total	99.77	100.30	100.05	99.87	99.59	99.25	98.85	98.50	100.94	101.05	101.25	99.53	100.68
Si	1.82	1.86	1.87	1.90	1.92	1.89	1.91	1.88	1.92	1.92	1.92	1.93	1.92
Al	0.22	0.18	0.16	0.12	0.08	0.12	0.11	0.13	0.09	0.12	0.11	0.06	0.09
Fe(ii)	0.17	0.15	0.20	0.21	0.21	0.26	0.25	0.26	0.30	0.31	0.33	0.25	0.28
Fe(iii)	0.15	0.13	0.11	0.11	0.09	0.13	0.10	0.15	0.08	0.06	0.07	0.10	0.10
Cr	0.00	0.00	0.00	0.00	0.00	0.00	0.00	0.00	0.00	0.00	0.00	0.00	0.00
Ti	0.03	0.02	0.03	0.02	0.02	0.02	0.02	0.02	0.02	0.02	0.01	0.01	0.01
Mn	0.01	0.01	0.01	0.01	0.01	0.01	0.01	0.01	0.01	0.01	0.01	0.01	0.01
Mg	0.78	0.82	0.81	0.84	0.86	0.77	0.81	0.77	0.80	0.75	0.75	0.81	0.76
Ca	0.84	0.85	0.82	0.80	0.81	0.81	0.81	0.79	0.77	0.79	0.79	0.83	0.83
Na	0.03	0.03	0.03	0.03	0.02	0.03	0.02	0.03	0.02	0.03	0.03	0.02	0.02
Total	4.05	4.04	4.03	4.03	4.05	4.04	4.03	4.05	4.04	4.04	4.03	4.03	4.03
Wo	43.22	43.36	42.23	40.79	40.91	40.73	40.76	39.81	39.29	40.89	40.33	41.59	41.57
En	40.01	41.86	41.49	42.82	43.04	38.55	40.70	38.67	40.52	38.90	38.32	40.18	38.49
Fs	16.78	14.78	16.28	16.40	16.05	20.71	18.54	21.53	20.20	20.21	21.35	18.23	19.93

Grain: P, phenocryst; GM, groundmass; INC, inclusion (mineral included within is stated in parentheses);
*mantling orthopyroxene.
Spot: C, core; M, mid point; R, rim.
Wo, wollastonite; En, enstatite; Fs, ferrosilite
Structural formula based on 6 oxygens.

Supplementary Table 4. Representative orthopyroxene mineral data

Sample Grain Position	G11 P1	G11 P2	G17 P1	G17 P2	G22 P1 C	G22 P2 C	G22 P3 R	G23 P1 C	G23 P1 R	G24 P1* (cpx P1) C	G24 P2* (cpx P2) C	G24 P3	G24 P4
SiO ₂	51.99	50.98	51.58	51.87	53.36	52.95	52.34	51.84	52.24	52.88	51.21	52.95	52.21
TiO ₂	0.29	0.29	0.27	0.21	0.21	0.17	0.26	0.32	0.26	0.16	0.33	0.23	0.29
Al ₂ O ₃	1.33	1.48	1.06	0.93	0.75	0.64	1.30	1.06	0.91	0.73	1.96	0.98	1.90
Cr ₂ O ₃	0.00	0.00	0.00	0.00	0.00	0.00	0.00	0.00	0.00	0.00	0.00	0.01	0.00
Fe ₂ O ₃	1.74	3.13	2.74	2.60	1.90	2.36	1.97	2.38	1.21	2.07	3.74	1.84	2.48
FeO	21.36	20.73	18.91	18.36	16.85	16.39	17.69	18.39	20.60	18.34	16.28	18.72	16.91
MnO	0.71	0.66	0.80	0.79	0.52	0.56	0.62	0.65	0.68	0.71	0.63	0.71	0.61
MgO	21.33	20.98	22.49	23.15	24.95	24.96	23.85	23.07	22.15	23.58	23.66	23.42	24.02
CaO	1.62	1.74	1.57	1.39	1.62	1.53	1.43	1.52	1.51	1.65	1.78	1.77	1.76
Na ₂ O	0.05	0.04	0.02	0.00	0.01	0.01	0.04	0.03	0.00	0.04	0.03	0.01	0.02
K ₂ O	0.00	0.00	0.00	0.00	0.00	0.00	0.00	0.00	0.00	0.00	0.00	0.00	0.00
NiO	0.01	0.00	0.01	0.02	0.00	0.00	0.01	0.00	0.01	0.00	0.00	0.00	0.00
Total	100.43	100.04	99.43	99.30	100.17	99.57	99.50	99.27	99.57	100.14	99.61	100.65	100.21
Si	1.95	1.93	1.94	1.95	1.96	1.96	1.95	1.96	1.91	1.96	1.91	1.96	1.93
Al	0.06	0.07	0.05	0.04	0.03	0.03	0.06	0.04	0.27	0.03	0.09	0.04	0.08
Fe(ii)	0.67	0.65	0.59	0.57	0.52	0.50	0.55	0.64	0.75	0.57	0.50	0.58	0.52
Fe(iii)	0.05	0.09	0.08	0.07	0.05	0.07	0.05	0.03	0.00	0.06	0.10	0.05	0.07
Cr	0.00	0.00	0.00	0.00	0.00	0.00	0.00	0.00	0.00	0.00	0.00	0.00	0.00
Ti	0.01	0.01	0.01	0.01	0.01	0.00	0.01	0.01	0.01	0.00	0.01	0.01	0.01
Mn	0.02	0.02	0.03	0.03	0.02	0.02	0.02	0.02	0.02	0.02	0.02	0.02	0.02
Mg	1.19	1.18	1.26	1.30	1.37	1.38	1.32	1.24	0.90	1.30	1.32	1.29	1.32
Ca	0.07	0.07	0.06	0.06	0.06	0.06	0.06	0.06	0.08	0.07	0.07	0.07	0.07
Na	0.00	0.00	0.00	0.00	0.00	0.00	0.00	0.00	0.00	0.00	0.00	0.00	0.00
Total	4.01	4.02	4.02	4.02	4.02	4.02	4.02	4.01	3.95	4.02	4.03	4.01	4.02
Wo	3.27	3.51	3.13	2.76	3.17	3.00	2.84	3.04	3.03	3.25	3.54	3.49	3.49
En	59.75	58.74	62.51	64.07	67.85	67.99	66.08	64.11	61.96	64.71	65.32	64.21	66.16
Fs	36.98	37.76	34.36	33.17	28.98	29.00	31.08	32.85	35.00	32.04	31.15	32.30	30.35

Sample Grain Position	G27 P2	G37A P2	G37A P3	G37A P4	G40 P1	G40 P2	G40 GM	G41 P1	G41 P2	G44 P1 C-M	G44 P1 R	G44 INC (CPX)	G44 P2
SiO ₂	51.62	52.26	52.62	51.87	51.30	51.45	51.14	53.25	52.94	53.60	53.37	53.31	52.78
TiO ₂	0.32	0.25	0.28	0.29	0.21	0.18	0.32	0.29	0.36	0.23	0.25	0.29	0.34
Al ₂ O ₃	1.49	0.90	1.12	1.68	0.59	0.89	1.06	1.73	1.58	1.40	1.97	1.51	1.12
Cr ₂ O ₃	0.00	0.00	0.01	0.00	0.00	0.00	0.00	0.01	0.01	0.01	0.00	0.00	0.00
Fe ₂ O ₃	3.11	2.75	2.23	2.14	3.26	2.62	3.46	1.68	1.48	0.76	1.22	2.12	1.33
FeO	16.99	17.67	18.39	19.09	17.97	21.13	17.03	16.26	17.73	18.11	16.13	15.22	19.10
MnO	0.64	0.71	0.70	0.60	0.78	0.85	0.71	0.52	0.59	0.51	0.46	0.50	0.73
MgO	23.53	23.67	23.44	22.69	22.65	21.03	22.66	25.15	24.02	24.49	25.55	25.89	22.99
CaO	1.76	1.59	1.61	1.58	1.79	1.57	2.45	1.68	1.81	1.50	1.35	1.59	1.88
Na ₂ O	0.04	0.02	0.05	0.03	0.02	0.04	0.03	0.04	0.03	0.02	0.04	0.02	0.04
K ₂ O	0.00	0.00	0.00	0.00	0.00	0.00	0.00	0.00	0.00	0.00	0.00	0.00	0.00
NiO	0.00	0.00	0.00	0.00	0.00	0.00	0.01	0.01	0.02	0.00	0.03	0.02	0.00
Total	100.04	99.81	100.46	99.96	99.77	98.88	100.61	100.43	100.04	100.62	100.36	100.48	100.31
Si	1.93	1.95	1.95	1.94	1.95	1.95	1.94	1.94	1.94	1.96	1.94	1.94	1.96
Al	0.07	0.04	0.05	0.07	0.03	0.04	0.05	0.07	0.07	0.06	0.08	0.06	0.05
Fe(ii)	0.53	0.55	0.57	0.59	0.57	0.67	0.53	0.49	0.54	0.55	0.49	0.46	0.59
Fe(iii)	0.09	0.08	0.06	0.06	0.09	0.07	0.10	0.05	0.04	0.02	0.03	0.06	0.04
Cr	0.00	0.00	0.00	0.00	0.00	0.00	0.00	0.00	0.00	0.00	0.00	0.00	0.00
Ti	0.01	0.01	0.01	0.01	0.01	0.01	0.01	0.01	0.01	0.01	0.01	0.01	0.01
Mn	0.02	0.02	0.02	0.02	0.03	0.03	0.02	0.02	0.02	0.02	0.01	0.02	0.02
Mg	1.31	1.32	1.29	1.26	1.28	1.19	1.28	1.37	1.31	1.33	1.39	1.41	1.27
Ca	0.07	0.06	0.06	0.06	0.07	0.06	0.10	0.07	0.07	0.06	0.05	0.06	0.07
Na	0.00	0.00	0.00	0.00	0.00	0.00	0.00	0.00	0.00	0.00	0.00	0.00	0.00
Total	4.02	4.02	4.02	4.02	4.02	4.03	4.01	4.01	4.02	4.01	4.01	4.02	4.01
Wo	3.49	3.14	3.17	3.16	3.57	3.16	4.88	3.30	3.58	2.96	2.66	3.09	3.75
En	65.05	64.95	64.43	63.21	62.88	58.85	62.90	68.75	66.15	67.32	70.16	70.21	63.67
Fs	31.46	31.92	32.39	33.63	33.54	38.00	32.22	27.95	30.27	29.72	27.18	26.70	32.58

Sample Grain Position	G48 P1	G48 P2	G48 P3	G48 P4	G49 GM	G49 P1	G49 P2	G49 P2	G49 P3	G49 GLOM	G49 GLOM	G51 L P1	G51 L P2
SiO ₂	52.57	54.04	52.52	53.05	53.11	52.90	52.16	52.42	52.36	52.58	53.26	51.47	51.07
TiO ₂	0.28	0.21	0.31	0.29	0.17	0.23	0.09	0.13	0.16	0.11	0.12	0.26	0.37
Al ₂ O ₃	1.30	0.62	0.80	0.80	0.41	0.96	0.38	0.43	0.63	0.54	0.54	1.14	0.92
Cr ₂ O ₃	0.02	0.00	0.02	0.00	0.04	0.00	0.00	0.00	0.00	0.00	0.00	0.01	0.01
Fe ₂ O ₃	2.05	0.32	1.97	1.01	0.00	0.00	2.09	2.09	1.31	1.26	0.31	2.49	2.06
FeO	17.48	19.87	19.98	21.15	23.44	23.05	20.77	21.26	21.96	21.86	22.90	21.83	21.41
MnO	0.60	0.65	0.64	0.74	0.89	0.85	0.97	0.92	0.98	0.91	0.95	0.88	0.79
MgO	24.00	23.51	22.48	21.88	20.77	20.94	21.94	21.85	21.48	21.66	21.56	20.77	20.51
CaO	1.53	1.76	1.76	2.02	1.43	1.46	1.13	1.16	1.11	1.10	1.08	1.43	1.95
Na ₂ O	0.06	0.03	0.03	0.05	0.03	0.01	0.03	0.04	0.02	0.03	0.03	0.04	0.03
K ₂ O	0.00	0.00	0.00	0.00	0.01	0.00	0.00	0.00	0.00	0.00	0.00	0.00	0.00
NiO	0.00	0.01	0.00	0.00	0.01	0.01	0.03	0.00	0.00	0.01	0.00	0.03	0.01
Total	99.50	98.56	99.77	98.88	100.61	100.57	100.62	100.30	100.00	100.07	100.74	100.34	99.12
Si	1.95	1.98	1.96	1.97	1.99	1.98	1.97	1.97	1.97	1.97	1.98	1.95	1.95
Al	0.06	0.03	0.04	0.04	0.02	0.04	0.02	0.02	0.03	0.02	0.02	0.05	0.04
Fe(ii)	0.54	0.61	0.62	0.65	0.74	0.72	0.65	0.66	0.69	0.68	0.71	0.69	0.68
Fe(iii)	0.06	0.01	0.05	0.03	0.00	0.00	0.06	0.06	0.04	0.04	0.01	0.07	0.06
Cr	0.00	0.00	0.00	0.00	0.00	0.00	0.00	0.00	0.00	0.00	0.00	0.00	0.00
Ti	0.01	0.01	0.01	0.01	0.00	0.01	0.00	0.00	0.00	0.00	0.00	0.01	0.01
Mn	0.02	0.02	0.02	0.02	0.03	0.03	0.03	0.03	0.03	0.03	0.03	0.03	0.03
Mg	1.32	1.28	1.25	1.21	1.16	1.17	1.24	1.22	1.20	1.21	1.20	1.17	1.17
Ca	0.06	0.07	0.07	0.08	0.06	0.06	0.05	0.05	0.04	0.04	0.04	0.06	0.08
Na	0.00	0.00	0.00	0.00	0.00	0.00	0.00	0.00	0.00	0.00	0.00	0.00	0.00
Total	4.02	4.03	4.02	4.03	4.01	4.01	4.01	4.02	4.01	4.01	4.00	4.02	4.02
Wo	3.04	3.47	3.50	4.01	2.89	2.97	2.26	2.30	2.23	2.21	2.16	2.88	3.97
En	66.24	64.50	61.99	60.62	58.57	59.12	61.05	60.49	60.05	60.45	60.11	58.14	58.03
Fs	30.72	32.02	34.51	35.37	38.53	37.91	36.70	37.21	37.72	37.33	37.73	38.98	38.00

Grain: P, phenocryst; GM, groundmass; INC, inclusion (mineral included within is stated in parentheses);
*mantled by clinopyroxene; GLOM, glomerocryst.
Spot: C, core; M, mid point; R, rim.
Wo, wollastonite; En, enstatite; Fs, ferrosilite
Structural formula based on 6 oxygens.

Supplementary Table 5. Olivine mineral data

Sample	G01B	G01B	G01B	G01B	G23	G26	G26	G26	G26	G26
Grain	P1	P1	P2	P3	P1	P1	P2	P2	P3	P4
Position	C	R	C				C	R		C
SiO ₂	36.25	36.67	36.72	36.86	36.96	34.87	34.73	35.38	35.65	35.30
TiO ₂	0.02	0.02	0.02	0.02	0.02	0.02	0.02	0.03	0.02	0.02
Al ₂ O ₃	0.00	0.00	0.00	0.00	0.00	0.00	0.00	0.00	0.00	0.00
Cr ₂ O ₃	0.00	0.00	0.01	0.01	0.00	0.00	0.00	0.00	0.00	0.00
MgO	36.13	36.15	35.82	36.01	35.29	26.44	27.00	27.12	31.85	27.74
CaO	0.11	0.13	0.13	0.12	0.14	0.20	0.18	0.17	0.15	0.16
MnO	0.51	0.50	0.51	0.54	0.54	0.82	0.86	0.86	0.68	0.82
FeO	26.57	27.06	26.79	26.30	27.54	37.43	37.44	38.15	31.94	36.17
NiO	0.02	0.01	0.01	0.03	0.00	0.01	0.00	0.01	0.01	0.04
Na ₂ O	0.02	0.02	0.00	0.02	0.00	0.02	0.00	0.00	0.01	0.00
K ₂ O	0.00	0.00	0.00	0.00	0.00	0.00	0.00	0.00	0.00	0.00
Total	99.63	100.56	100.00	99.88	100.50	99.80	100.23	101.71	100.32	100.24
Si	0.97	0.98	0.98	0.98	0.99	0.99	0.98	0.98	0.98	0.99
Al	0.00	0.00	0.00	0.00	0.00	0.00	0.00	0.00	0.00	0.00
Fe(ii)	0.60	0.60	0.60	0.59	0.61	0.89	0.88	0.89	0.73	0.85
Mn	0.01	0.01	0.01	0.01	0.01	0.02	0.02	0.02	0.02	0.02
Mg	1.45	1.43	1.43	1.43	1.40	1.12	1.14	1.12	1.30	1.16
Ca	0.00	0.00	0.00	0.00	0.00	0.01	0.01	0.01	0.00	0.00
Total	3.03	3.03	3.02	3.02	3.02	3.02	3.02	3.02	3.03	3.02
Fo	70.8	70.4	70.5	70.9	69.6	55.7	56.2	55.9	64.0	57.8
Fa	29.2	29.6	29.5	29.1	30.4	44.3	43.8	44.1	36.0	42.2

Sample	G26	G30	G30	G35	G35	G35	G51 D	S106B	S106B	S106B
Grain	P4	P1	P2	P1	P2	P3	P1	INC	P1	P2
Position	R								M	M
SiO ₂	34.40	36.02	35.39	34.98	35.69	36.07	37.42	36.27	35.28	35.09
TiO ₂	0.04	0.01	0.02	0.02	0.02	0.02	0.03	0.01	0.04	0.02
Al ₂ O ₃	0.00	0.00	0.00	0.00	0.00	0.00	0.00	0.00	0.00	0.00
Cr ₂ O ₃	0.02	0.00	0.00	0.00	0.00	0.01	0.01	0.00	0.00	0.00
MgO	26.80	33.48	30.56	29.75	31.14	32.77	36.18	32.79	28.36	27.32
CaO	0.19	0.17	0.15	0.21	0.19	0.23	0.14	0.17	0.19	0.19
MnO	0.86	0.53	0.58	0.67	0.64	0.59	0.42	0.58	0.81	0.82
FeO	37.26	29.83	32.65	33.88	32.41	30.74	26.38	29.60	35.56	36.65
NiO	0.01	0.01	0.00	0.02	0.01	0.02	0.01	0.01	0.00	0.01
Na ₂ O	0.01	0.00	0.03	0.04	0.00	0.01	0.02	0.01	0.02	0.01
K ₂ O	0.00	0.00	0.00	0.00	0.00	0.00	0.00	0.00	0.00	0.00
Total	99.59	100.06	99.39	99.58	100.11	100.45	100.61	99.44	100.24	100.10
Si	0.98	0.98	0.98	0.98	0.98	0.98	0.99	0.99	0.98	0.99
Al	0.00	0.00	0.00	0.00	0.00	0.00	0.00	0.00	0.00	0.00
Fe(ii)	0.89	0.68	0.76	0.79	0.75	0.70	0.58	0.67	0.83	0.86
Mn	0.02	0.01	0.01	0.02	0.01	0.01	0.01	0.01	0.02	0.02
Mg	1.14	1.35	1.26	1.24	1.28	1.33	1.43	1.33	1.18	1.14
Ca	0.01	0.01	0.00	0.01	0.01	0.01	0.00	0.00	0.01	0.01
Total	3.03	3.03	3.02	3.03	3.02	3.03	3.01	3.02	3.02	3.02
Fo	56.2	66.7	62.5	61.0	63.1	65.5	71.0	66.39	58.71	57.06
Fa	43.8	33.3	37.5	39.0	36.9	34.5	29.0	33.61	41.29	42.94

Grain: P, phenocryst; INC, inclusion.
Spot: C, core; M, mid point; R, rim.
Fo, forsterite; Fa, fayalite

Supplementary Table 6. Representative Fe-Ti oxide mineral data

Sample	G01B	G01B	G01B	G01B	G11	G11	G17	G17	G22	G22	G23	G23	G26
Grain Position	INC	GM	P1 C	P1 R	P1	P2	INC (OPX)	P1	P1 C	INC (OPX)	GM	INC (CPX)	P1
SiO ₂	0.03	0.07	0.06	0.05	0.05	0.06	0.06	0.06	0.03	0.05	0.04	0.08	0.07
TiO ₂	10.22	10.44	10.51	10.50	12.18	11.34	11.28	12.22	11.80	10.90	8.74	11.55	11.43
Al ₂ O ₃	4.63	4.26	4.31	4.25	2.28	2.98	2.48	1.30	2.86	3.10	5.54	4.04	3.90
Cr ₂ O ₃	0.19	0.09	0.11	0.13	0.09	0.08	0.04	0.09	0.04	0.06	0.08	0.07	0.05
Fe ₂ O ₃	45.61	44.64	44.48	44.77	43.39	44.12	44.79	43.05	43.44	44.56	47.00	43.28	42.78
FeO	35.17	35.32	35.40	35.42	38.40	38.10	39.41	40.91	38.98	37.71	33.65	37.10	39.13
MnO	0.42	0.36	0.31	0.40	0.44	0.44	0.50	0.46	0.48	0.36	0.29	0.36	0.45
MgO	3.76	3.53	3.61	3.56	2.45	2.24	1.36	0.59	1.91	2.19	3.90	3.19	1.78
CaO	0.02	0.07	0.00	0.02	0.00	0.01	0.00	0.01	0.00	0.02	0.02	0.12	0.00
Total	100.05	98.77	98.79	99.09	99.28	99.37	99.92	98.68	99.54	98.96	99.27	99.79	98.77
Si	0.01	0.02	0.02	0.01	0.02	0.02	0.02	0.02	0.01	0.02	0.01	0.02	0.02
Ti	2.22	2.30	2.32	2.31	2.72	2.53	2.53	2.80	2.63	2.44	1.91	2.53	2.54
Al	1.58	1.47	1.49	1.47	0.80	1.04	0.87	0.47	1.00	1.09	1.89	1.39	1.36
Cr	0.04	0.02	0.03	0.03	0.02	0.02	0.01	0.02	0.01	0.02	0.02	0.02	0.01
Fe(iii)	9.92	9.86	9.82	9.86	9.70	9.84	10.03	9.87	9.70	9.98	10.25	9.49	9.51
Fe(ii)	8.50	8.67	8.68	8.67	9.54	9.45	9.81	10.43	9.68	9.39	8.16	9.04	9.67
Mn	0.10	0.09	0.08	0.10	0.11	0.11	0.13	0.12	0.12	0.09	0.07	0.09	0.11
Mg	1.62	1.54	1.58	1.55	1.09	0.99	0.60	0.27	0.85	0.97	1.68	1.39	0.78
Ca	0.01	0.02	0.00	0.01	0.00	0.00	0.00	0.00	0.00	0.01	0.01	0.04	0.00
Total	24.00	24.00	24.00	24.00	24.00	24.00	24.00	24.00	24.00	24.00	24.00	24.00	24.00
TiO ₂	11.23	11.54	11.62	11.57	12.97	12.12	11.81	12.70	12.52	11.70	9.78	12.56	12.25
Fe ₂ O ₃	50.12	49.38	49.22	49.37	46.17	47.16	46.91	44.76	46.11	47.82	52.57	47.08	45.83
FeO	38.65	39.08	39.16	39.06	40.86	40.72	41.28	42.54	41.37	40.48	37.64	40.36	41.92

Sample	G30	G30	G30	G35	G35	G40	G44	G44	G48	G49	G51 L	G51 D	G51 D
Grain Position	INC (CPX)	P1 C	P1 R	P1	P2	P1	P1	P2	P1	GLOM	P1	P1 C	P1 R
SiO ₂	0.07	0.07	0.05	0.04	0.04	0.05	0.09	0.07	0.00	0.04	0.03	0.01	0.04
TiO ₂	11.72	12.80	12.86	15.23	18.48	12.37	9.83	9.99	0.97	12.27	13.44	12.92	12.86
Al ₂ O ₃	5.57	4.76	4.72	0.99	1.39	2.36	4.53	4.36	2.76	0.88	1.52	1.40	1.42
Cr ₂ O ₃	0.18	0.08	0.09	0.08	0.10	0.07	0.11	0.10	0.09	0.07	0.03	0.07	0.07
Fe ₂ O ₃	41.65	39.64	39.82	38.32	31.65	42.10	45.33	45.52	64.86	43.94	42.66	43.18	42.64
FeO	36.34	39.05	39.26	44.05	45.34	40.71	35.64	35.78	27.68	41.00	41.51	40.78	40.50
MnO	0.38	0.40	0.51	0.40	0.50	0.53	0.37	0.37	0.79	0.46	0.48	0.53	0.54
MgO	4.08	2.78	2.67	0.57	1.55	0.99	3.10	3.14	2.47	0.63	1.43	1.34	1.32
CaO	0.00	0.00	0.01	0.00	0.00	0.00	0.00	0.00	0.04	0.01	0.00	0.00	0.04
Total	99.97	99.59	99.99	99.99	99.68	99.19	99.00	99.33	99.09	99.29	99.59	99.99	99.68
Si	0.02	0.02	0.01	0.01	0.01	0.02	0.03	0.02	0.00	0.01	0.01	0.00	0.01
Ti	2.53	2.81	2.81	3.45	4.16	2.80	2.17	2.20	0.22	2.80	2.98	2.90	2.91
Al	1.88	1.63	1.62	0.35	0.49	0.84	1.57	1.50	0.97	0.32	0.53	0.49	0.50
Cr	0.04	0.02	0.02	0.02	0.02	0.02	0.03	0.02	0.02	0.02	0.01	0.02	0.02
Fe(iii)	8.98	8.69	8.71	8.70	7.14	9.52	10.01	10.03	14.57	10.04	9.47	9.69	9.64
Fe(ii)	8.71	9.52	9.54	11.11	11.36	10.23	8.75	8.76	6.91	10.41	10.24	10.17	10.18
Mn	0.09	0.10	0.12	0.10	0.13	0.13	0.09	0.09	0.20	0.12	0.12	0.13	0.14
Mg	1.74	1.21	1.16	0.26	0.69	0.44	1.36	1.37	1.10	0.29	0.63	0.60	0.59
Ca	0.00	0.00	0.00	0.00	0.00	0.00	0.00	0.00	0.01	0.00	0.00	0.00	0.01
Total	24.00	24.00	24.00	24.00	24.00	24.00	24.00	24.00	24.00	24.00	24.00	24.00	24.00
TiO ₂	13.06	13.99	13.99	15.60	19.36	12.99	10.82	10.94	1.04	12.62	13.77	13.33	13.40
Fe ₂ O ₃	46.43	43.33	43.31	39.27	33.16	44.23	49.92	49.86	69.36	45.20	43.71	44.57	44.41
FeO	40.51	42.68	42.70	45.13	47.49	42.77	39.25	39.19	29.60	42.18	42.52	42.10	42.19

Grain: P, phenocryst; GM, groundmass; GLOM, glomerocryst; INC, inclusion (mineral included within is stated in parentheses).
Spot: C, core; M, mid point; R, rim.
Structural formula based on 32 oxygens.

Supplementary Table 7. Distribution coefficients used in trace element modelling

	Olivine	Clinopyroxene	Orthopyroxene	Plagiocalse	Hornblende	Fe-Ti oxide
Sr	0.05	0.14	0.05	1.86	0.28	0.11
Ba	0.04	0.04	0.07	0.44	0.24	0.18
La	0.034	0.130	0.068	0.183	0.116	0.150
Eu	0.018	0.602	0.180	0.549	0.657	0.182
Yb	0.077	0.661	0.372	0.052	0.816	0.218
Ni	14.14	5.27	9.40	0.40	11.40	22.15
V	0.11	2.15	1.78	0.14	6.05	26.08
Nb	0.03	0.17	0.35	0.27	0.31	0.84

Data taken from the Geochemical Earth Reference Model (GERM) database:
<http://earthref.org/GERM/> for basalts to andesites, except hornblende La, Eu and Yb
values were taken from Bottazzi et al. 1999.